

Title of Thesis: CHARACTERIZATION AND FABRICATION OF
NOVEL RUTHENIUM OXIDE-ZINC BATTERIES

Author: Mahsa Dornajafi, Master of Science, 2010

Directed by: Professor Christopher Davis
Department of Electrical and Computer Engineering
University of Maryland - College Park

Ultrathin galvanic cells that can comply with a variety of form factors and electronic system packages are of tremendous technological importance. They show promise for application in flexible electronic systems. This Thesis describes a flexible, high energy density galvanic cell, based on hydrated ruthenium (IV) oxide-zinc electrodes utilizing $\text{RuO}_2 \cdot n\text{H}_2\text{O}$ nanoparticles in amounts that are not cost-prohibitive. This battery is suitable for use in a number of environments. It is non-toxic, environmentally friendly, and, based on aqueous electrolytes, it is safe in operation. It can be optimized for volume manufacture at low cost. As it functions at much lower cell voltage than Li-ion batteries, it can be recharged remotely, at conveniently low voltage, by harvesting, for example, radio-frequency (RF) energy. At present this cell demonstrates a specific capacity of over 50 mAh cm^{-2} . This is the largest capacity reported for thin-film cells. Also, its cycle life of up to 200 charge-discharge cycles is very promising for use as a secondary galvanic cell.

This Thesis focuses on (i) the optimization of anode and cathode materials, (ii) the identification of the composition of the electrolyte, (iii) the choice of the most suitable cell separator, and (iv) the elaboration of the most efficient assembly procedures.

CHARACTERIZATION AND FABRICATION OF NOVEL RUTHENIUM OXIDE-ZINC BATTERIES

by
Mahsa Dornajafi

Thesis submitted to the Faculty of Graduate School of the
University of Maryland, College Park, in partial fulfillment
of the requirement for the degree of
Master of Science
2010

Advising Committee:
Professor Christopher Davis (Chair)
Professor Martin Peckerar
Professor Neil Goldsman

Copyright © by
Mahsa Dornajafi
2010

Dedication

*I dedicate this dissertation to my parents and my brothers for all their support and love
which was my greatest inspiration in life.*

You always believed in me.

I Love you all

Acknowledgement

The accomplishment reported in this Thesis would not have been possible without significant help, contribution, and moral support received from my colleagues, friends, and family.

I would like to express my indebtedness and gratefulness to Professor Martin Peckerar for his guidance and assistance over that past 2 years. Also, I would like to thank my dissertation committee, Professor Christopher Davis, the Chair, and Professor Neil Goldsman.

I feel privileged for having collaborated with numerous talented individuals at FlexEl, LLC, and I would like to acknowledge my colleagues: Dr. Bob Proctor, Dr. Zeynep Dilli, Karina Drees, Vincent De Chacus, and Benjamin Krupsaw.

My special thanks go to Dr. Daniel Lowy for his sharing his insight in the chemical and electrochemical aspects of our battery system, for his support and encouragements. It was a real pleasure learning from him as a student, and working with him, as a colleague.

As a member of the Analog and mixed-signal Laboratory at University of Maryland, I would like to recognize my colleagues and friends: Kwangsik Choi, Filiz Yesilkoy, and Scott Bauman. I would like to thank the entire promise family at the Graduate School Office, University of Maryland.

And last but not least, I would like to express deep gratitude to my family. I thank my father for all his support, love, and care. I thank my mother, Marjaneh, for all those times when she stood by me, for having been my strength when I was weak, for her tireless love and support.

I would like to thank my brothers, Hamid Reza and Saeed. You are the best brothers that anyone could have. You are the reason that I can go on in my life.

I would like to thank my friend, Dr. Ali Izadi, for his support and care over my undergraduate years.

Thanks to Almighty God for giving me strength, health, and mental fortitude to successfully complete this Master's journey.

Sincerely,
Mahsa Dornajafi

CONTENTS

1. MOTIVATION AND BACKGROUND	1
1.1 Motivation	1
1.2 Goals and Accomplishment of This Thesis	4
1.3 Background	4
1.3.1 Thin-Film Lithium and Lithium-Ion Batteries	4
1.3.2 Flexible Zinc-Carbon Batteries	7
1.3.3 Flexible Hybrid Power Sources	10
1.3.4 Thin-Film Hydrated RuO ₂ Electrodes	10
2. THE ELECTROCHEMISTRY OF GALVANIC CELLS	13
2.1 Brief description of battery operation	13
2.2 Thermodynamic Considerations	14
2.2.1 Oxidation-Reduction Reactions	14
2.2.2 Electrochemical Potential	15
2.3 Kinetics of a Battery	17
2.3.1 Overpotential	17
2.4 Chemical and Physical Considerations of a Galvanic Cell	23
2.4.1 Electrolyte Effects	23
2.4.2 Separators	27
3. FABRICATION AND CHARACTERIZATION OF NOVEL ZINC-RUTHENIUM OXIDE CELLS	29
3.1 Chemical Considerations for Novel Zinc-Ruthenium Oxide Cell	29
3.1.1 Close Look at the Cathode Side	29

3.1.2	Close Look at the Anode Side	32
3.1.3	Close Look at the Cell Capacity	33
3.1.4	Initial Electrolyte Utilized in Zn – RuO _x Galvanic Cells	33
3.2	Physical Consideration and Fabrication of a Novel RuO ₂ Cell	35
3.2.1	Initial Separator Utilized in Zn – RuO _x Galvanic Cell	37
3.2.2	Thin Separators	37
3.2.3	Cathode Current Collectors	37
3.2.4	Anode Current Collectors	38
3.2.5	Anode in Zn – RuO _x Galvanic Cell	39
4.	EXPERIMENTAL TECHNIQUES	45
4.1	ELECTROCHEMICAL Instrumentation	45
4.1.1	Electrochemical Techniques Performed in 3-Electrode Geometry	47
4.1.2	Electrochemical Techniques Performed in 2-Electrode Geometry	47
4.2	Electrochemical Techniques and Testing Procedures	48
4.2.1	Cyclic Voltammetry (CV)	48
4.2.2	Open Circuit Voltage	48
4.2.3	Charge /Discharge Studies	49
4.2.4	Shelf Life/Self-Discharge	57
4.2.5	Internal Resistance	58
5.	MEASUREMENTS AND TESTING RESULTS	61
5.1	Electrolyte Effects Measurements	61
5.1.1	Original Electrolyte	61
5.1.2	Overview of Electrolytes of Different pH Value	62
5.2	Cathode Current Collector	65
5.3	Separator Analysis	65
5.4	Anode Materials	68
5.4.1	Zinc-RuO _x Batteries	68
5.4.2	Al – RuO _x Battery	70

5.5	Monitoring Hydrogen Discharge and Water Decomposition by Cyclic Voltammetry in Open Cell Experiments	70
5.6	XPS Analysis	73
5.6.1	Analysis on the Cathode Side	74
5.6.2	Analysis on the Anode Side	75
5.6.3	Further XPS Measurements and Analysis	76
6.	MANUFACTURING AND COST ANALYSIS OF Zn – RuO₂ BATTER- IES	81
6.1	Current Stage of the Novel Ruthenium(IV) Oxide Cells	81
6.1.1	Thickness	81
6.1.2	Capacity	82
6.1.3	Costs	83
6.1.4	Cycle Life	83
6.1.5	Safety and Sustainability	84
7.	ACCOMPLISHMENTS AND FUTURE CONSIDERATIONS	85
7.1	Summary of Main Accomplishments	85
7.2	Future Considerations	87
7.2.1	Anode Optimization	87
7.2.2	Cathode Optimization	87
7.2.3	Electrolyte Optimization	88

LIST OF TABLES

3.1	The anodic material used in batteries.	39
5.1	Denomination of different electrolytes with different pH value and the charge capacities enabled by them. All batteries were made under similar conditions and testing environment.	63
5.2	Different current collectors.	65
5.3	Nominal continuous current for different cathode current collectors	66
5.4	Different separators with different thickness and their performance in capacity, number of cycles, and internal resistance.	66
5.5	Potential windows for various electrolytes.	73
6.1	The Capacity Comparison of Non-Rechargeable Flexible Batteries.	82

LIST OF FIGURES

3.1	Constant load discharge of a 4cm^2 cell through $1\text{k}\Omega$ load.	34
3.2	(a)Top view of the battery. (b) Cross sectional view of battery.	35
3.3	Piece of a separator under the microscope.	41
4.1	Schematic of the potentiostat: the equivalent circuit of a 3-electrode cell (E_i is the input voltage, R_m - current-measuring resistor, and CA - control amplifier).	46
4.2	Principle of cyclic voltammetry. In the left bottom panel the applied potential is displayed vs. time, and the current response vs. time is shown above it, while the right panel shows the output, the voltammogram in which current is plotted relative to the applied potential.	49
4.3	European sign convention.	50
4.4	Constant current charging with $240\mu\text{A}$ current.	51
4.5	Constant current charging with $50\mu\text{A}$ current.	52
4.6	Constant voltage charge current of a Zn – RuO ₂ cell, when charged at 1.4V for 1h	52
4.7	Constant load discharge of a battery through $1\text{k}\Omega$ external load, providing a charge capacity of over $10\text{mAh}/\text{cm}^2$	53
4.8	Voltage vs. time discharge recorded by CP for calculating the internal resis- tance of a cell.	54
4.9	100 cycles accomplished from a 4cm^2 Zinc-RuO ₂ battery with 1k load and 1.4V charging intervals.	55
4.10	The capacity plot drawn from a 4cm^2 Zn-RuO ₂ battery	55
4.11	800 cycles accomplished by the Zn – RuO ₂ battery.	56

4.12	Three-month discharge of a cell with 16cm^2 of active area, operating with electrolyte of near neutral pH.	57
4.13	Two months discharge of a 5V cell with 4cm^2 of active area and acidic pH.	58
4.14	The equivalent circuit of a battery.	59
4.15	Calculating the internal resistance of a cell by using CP technique; it yields the value of 5Ω	60
5.1	Plot of battery capacity versus pH for different electrolytes. Note that connecting point is just for visual clarity.	62
5.2	Capacity versus different pH values of the electrolytes that belong to the same family; they all contain different concentrations of zinc chloride and ammonium chloride. Note that connecting point is just for visual clarity.	64
5.3	Capacity versus the thickness of a separator obtained from Zinc-RuO ₂ battery system. Note that connecting point is just for visual clarity.	67
5.4	Number of cycles versus the thickness of a separator obtained from the Zn – RuO ₂ battery system. Note that connecting point is just for visual clarity.	67
5.5	Internal resistance of a cell versus the different separators thickness. Note that connecting point is just for visual clarity.	68
5.6	Discharge curve for Zn – RuO ₂ battery with pH2.48 electrolyte over $1\text{k}\Omega$ load	69
5.7	Approximately 100 cycles accomplished with Zn – RuO ₂ battery through $1\text{k}\Omega$ load with charging cycle in between two discharges, at an applied voltage of 1.4V	69
5.8	(a). Discharge curve for the Al – RuO ₂ battery with pH6.2 electrolyte. (b). Discharge curve for the Al – RuO ₂ battery with pH0.2.	70
5.9	CV scans recorded for electrolyte E10A5, at 100mV/s : inner (blue) scan: from -1.05V to $+1.22\text{V}$ vs. Ag(RE), while the external curve was obtained in the potential range from -1.05V to $+1.22\text{V}$ vs. Ag (RE).	72
5.10	The Si(2p) peak obtained with XPS.	74
5.11	Full XPS spectrum for cathode-side samples from undischarged (top) and discharged (bottom) batteries.	77

5.12	Top: Zoom in on the C1s/Ru3d peak; left: new battery; right: discharged battery. Bottom: Zoom in on the Ru3p split peak; left: new battery; right: discharged battery. Of the four peaks visible in the bottom left graph, from left to right (higher-to-lower binding energy) the peaks are Zn Auger, Ru 1p, Zn Auger, the other Ru 1p. In the discharged battery graph, only the Zn peaks remain clearly visible.	78
5.13	Full XPS spectrum for anode-side (Zn) samples from undischarged (top) and discharged (bottom) batteries.	79
5.14	Zoom in on the Zn2p peaks from the new (left) and discharged (right) batteries.	79
5.15	Piece of a separator under the microscope.	80

Chapter 1

MOTIVATION AND BACKGROUND

“Imagine a world without batteries! A teenager walks outside wearing headphones, tethered to home by a lengthy extension cord. An old man winds his pacemaker like a pocket watch. In thousands of ways, large and small, batteries have changed our daily lives.”

Mary Ellen Bowden, *Chemistry is Electric!* (Chemical Heritage Foundation, Philadelphia, 1997), p.26.

1.1 Motivation

Modern life has become progressively more mobile, and therefore dependent on the availability of portable power sources. In recent years there has been a rapid increase in the use of battery operated devices, such as cell phones, Blackberries, laptops, iPods, remote car lock controls, wall clocks, toys, and remote controls for TV, DVD, or CD players [1, 3]. According to statistical accounts, at present an average person in an industrialized country consumes as many as 35 batteries a year. In the United States the market for batteries grows at 6% annually, and was expected to reach \$15 billion in 2009[4, 5]. According to forecasts, the global battery demand will increase 4.8% annually through 2012. China will record the largest gains, and will likely surpass the U.S. as the largest market. Consumer battery demand will outperform the market as a whole; non-lead-acid secondary battery market gains will outpace the demand for primary and lead-acid secondary batteries [4].

Rising demand for portable nanoelectronic devices triggers today’s unprecedented development of dimensionally small batteries [2, 6, 7]. In order to maintain adequate operation

time of portable devices, which are becoming increasingly powerful and power hungry, the consumer market demands small size batteries with high energy density as well as a reasonable runtime and longevity [8, 9, 10].

By definition, a battery is an assembly of single electrochemical or voltaic cells, connected in series or parallel, which convert energy evolved in chemical reactions into low-voltage, direct current electricity. It consists of a positive electrode (the cathode) and a negative electrode (the anode), separated by an electrolyte, which is generally a liquid solution containing a salt dissolved in a solvent, and is imbedded in a felt (the separator). All these components are involved in electrochemical charge transfer reactions, which proceed at the interface between the electrodes and the electrolyte. These reactions convert chemical energy into electric energy, so that they can power various loads placed in the external circuit. As most charge transfer reactions are reversible, secondary cells can be recharged by electricity supplied from an external power source [11, 12]. Going into more detail, at the anode electrons are generated to do external work. In lithium-ion batteries the anode contains lithium, commonly held within graphite. The cathode is the electronegative electrode to which electrons migrate through the external electrical circuit, while positive ions migrate inside the cell. Hence, the role of the electrolyte is to allow the flow of ions (e.g., Li^+ ions, protons, hydroxide ions, etc.) from one electrode to another. One important requirement for the electrolyte is to be stable in the presence of both electrodes. Inert current collectors allow the transport of electrons to and from the electrodes. They are typically metals, which do not react with the electrode materials; in most cases, copper is used for the anode and aluminum for the cathode [13].

Existing thin-film battery technologies have severe cost and performance limitations, which hinder the efficient use of the device. Future utilization of electrical energy, with a greater emphasis on renewable energy sources, depends on the development of the next generation of batteries. As of today, limited energy storage capacity of individual battery cells and the lack of fast recharge cycles with long cell lifetimes represent additional restrictions. In order to improve the energy storage capacity of a given cell significantly, one needs to increase the cell voltage and/or the amount of charge stored reversibly per unit mass and volume. These requirements call for the exploration of new materials with nanoscale

features that could enhance reversible charge storage [5].

Over the past two decades solid-state thin-film lithium and lithium-ion batteries have been developed. Many of these systems were rechargeable, and exhibit long cycle lives. They have been devised with a variety of electrode materials and in different cell configurations, on thin ceramic, metal, or silicon substrates [14]. The goal of this Thesis is to show how to build fully flexible and robust electrochemical cells. This requires multiple components with specific electrochemical and interfacial properties to be integrated into single units. These basic components, i.e., the electrodes, separator, and electrolyte, can all be integrated into single contiguous nano-composite units, which can then serve as building blocks for a variety of thin mechanically flexible energy storage devices [15]. In previous works, such batteries have been less than $15 \mu\text{m}$ thick, and have important applications in a variety of consumer and medical products. Cells with crystalline LiCoO_2 cathodes can deliver up to 30% of their maximum capacity between 4.2 and 3 V at discharge currents of $10\text{mA}/\text{cm}^2$. At lower discharge-charge cycle rates, the capacity decreases by negligible amounts over thousands of cycles [16]. According to literature reports, prototype thin-film batteries fabricated with crystalline LiCoO_2 cathode consistently provide the power levels up to $30\text{mW}/\text{cm}^2$. They exhibit long cycle life, negligible self-discharge, and rapid charge rates [17]. Nevertheless, none of the commercially available thin-film cells possess such high energy densities; lithium thin-film batteries typically provide substantially less than $1\text{mAh}/\text{cm}^2$ capacity [18]. Promising results have also been obtained with crystalline LiMn_2O_4 cathodes, although no good reproducibility has been achieved with this system [17]. A viable approach toward flexible power systems consisted in utilizing as the electrodes nonporous cellulose paper embedded with aligned carbon nanotubes. Such building blocks have been used for devising flexible supercapacitors, batteries, and hybrid power systems, as well as dual-storage battery-in-supercapacitor devices. It was demonstrated that thin freestanding nano-composite paper devices offer complete mechanical flexibility during operation. Hence, these easy-to-assemble integrated nanocomposite energy-storage systems could provide unprecedented design freedom for a variety of devices operating over a wide range of temperature and environmental conditions [15]. Other very promising electrode supports are polypyrrole films. They can be prepared by electrochemical polymerization

methods, and are obtained as highly flexible and bendable free-standing films. These battery components look paper-like, are soft, lightweight, mechanically robust, and exhibit high electrical conductivity. Such free-standing films show promise as cathodes for flexible and bendable batteries [19].

1.2 Goals and Accomplishment of This Thesis

In this thesis I present the first systematic evaluation of a cathode electrode containing ruthenium oxide used in a thin-film flexible galvanic cell. I describe the impact of varying different component parameters for this battery, such as: electrolyte pH, separator material, and the electrode current collector materials.

I have found that each of the parameters studied proved optimal in the sense disclosed:

- Electrolyte pH of 2.48 gives the highest cell capacity.
- The fiber-glass separator gives the highest cell capacity and provides lowest internal resistance. However, this separator has the highest thickness as compared to other separators studied.
- Different materials have been tested as cathode current collectors for optimizing the cell. The 0.13 mm thick graphite sheet has been chosen as the current collector for its low cost, low internal resistance and high continuous current. Depending on our applications and limitations different cathode current collector can be used.

The finished, optimized product, provides a capacity $> 20\text{mAh}/\text{cm}^2$. This is the highest thin film battery storage capacity reported in open literature.

1.3 Background

1.3.1 Thin-Film Lithium and Lithium-Ion Batteries

These galvanic cells belong to several types, according to their cathode materials. Cathodes utilized in these batteries include crystalline or nano-crystalline oxide-based lithium intercalation compounds. Anodes are made of lithium metal, inorganic compounds, e.g.,

silicon-tin oxynitrides, Sn_3N_4 , and Zn_3N_2 , or metal films, such as Cu, in which the anode is formed by lithium plating on the initial charging. Typically, the electrolyte is a glassy lithium phosphorus oxynitride (“Lipon”) [13].

The construction and testing of batteries that operate with cathodes made of (i) LiCoO_2 , (ii) LiMnO_2 , and (iii) $\text{Li}_8\text{V}_2\text{O}_5$, or (iv) hydrated RuO_2 appear in literature [20, 21, 22]. The latter being utilized mainly as electrode materials for supercapacitors. We will briefly review the manufacturing, testing, and performance of such galvanic cells.

So-called “Li-free” thin-film batteries have the following cell configuration: Li diffusion blocking overlayer/Cu/solid lithium electrolyte (Lipon)/ LiCoO_2 . These cells are activated during the initial charge by in situ plating of metallic Li onto the Cu anode current collector. Electrochemical cycling between 4.2 and 3.0 V was demonstrated for a number of over 1000 cycles, at the current density of $1\text{mA}/\text{cm}^2$ or for 500 cycles at $5\text{mA}/\text{cm}^2$. The overlayer confers high cycle stability; otherwise the plated Li rapidly develops a detrimental morphology, and the battery loses most of its capacity within a few cycles. Li-free thin-film batteries retain their high cell voltage, while permitting a simple fabrication process in air, thus avoiding problems related to the presence of a metallic Li anode [20].

The performance of lithium-ion thin-film batteries could be improved by heat treatment (at 250°C in air for 1h). Cells consisted of an amorphous silicon tin oxynitride anode (‘SiTON’), an amorphous lithium phosphorus oxynitride electrolyte (‘Lipon’), and a crystalline LiCoO_2 cathode. They sustained the capacity of $5\text{mA}/\text{cm}^2$ in the voltage range from 4.2 to 2.7 V. Long-term cycling stability test of a SiTON/Lipon/ LiCoO_2 batteries (between 3.93 and 2.7 V) demonstrated that their capacity faded only by 0.001% per cycle [21].

Thin-film rechargeable lithium batteries with amorphous and crystalline LiCoO_2 cathodes were investigated. The lithium cobalt oxide films were deposited by radio-frequency (RF) magnetron sputtering of a LiCoO_2 target in a 3:1 Ar/ O_2 mixture gas. From proton-induced gamma-ray emission analysis (PIGE) and Rutherford backscattering spectrometry (RBS), the average composition of these films was determined to be $\text{Li}_{1.15}\text{CoO}_2$ [15] or, within experimental uncertainty, $\text{LiCoO}_2 + 0.08\text{Li}_2\text{O}$. The x-ray powder diffraction patterns of films annealed in air at 500 to 700°C were consistent with the regular hexagonal

structure observed for crystalline LiCoO_2 . The discharge curves of the cells with amorphous LiCoO_2 cathodes showed no obvious structural transition between 4.2 and 2.0V, while the discharge curves of the cells with polycrystalline cathodes were consistent with a two-phase potential plateau at ~ 3.9 V with a relatively large capacity. Two lower capacity plateaus were observed at ~ 4.2 and 4.1 V with the 600 and 700°C annealed cathodes; the $-dq/dV$ peaks were broader and weaker for the 600°C annealed cathodes and were not present at all with the 500°C annealed films. The chemical diffusion coefficients of Li^+ in the cathodes obtained from ac impedance measurements at cell potentials of ~ 4 V ranged from $\sim 10 - 12\text{cm}^2/\text{s}$ for the as-deposited amorphous cathodes to $\sim 10 - 9\text{cm}^2/\text{s}$ for the films annealed at 700°C . The capacity loss on extended cycling of the thin-film cells varied with the crystallinity and thickness of the cathodes and with temperature. With the highly crystalline, 700°C annealed material, losses on cycling between 4.2 and 3.8V at 25°C ranged from 0.0001%/cycle (> 104 cycles) to 0.002%/cycle for cells with cathodes from $0.05\mu\text{m}$ to $0.5\mu\text{m}$ thick [22].

Thin-film cathodes consisting of crystalline lithium manganese oxide with the general composition $\text{Li}_{1+x}\text{Mn}_{2-y}\text{O}_4$ enabled for extended cycling of lithium cells, at the temperatures of 25 and 100°C [16]. Innovative electrolyte materials, such as polymers or inorganic glasses, allow for designing flat lithium primary or secondary batteries. The so-called "hybrid plastic electrolytes" enable for devising thick film cells (with the thickness in the range of $1\text{mm}-3\text{mm}$) that possess a specific surface capacity of several mAh cm^{-2} . Secondary Li-ion batteries typically last less than 500 cycles. By contrast, all solid state thin-film batteries offer better cycleability and exhibit liquid leakage. Their specific surface capacity is, however, about one order of magnitude lower than for the polymer electrolyte batteries. Solid cells can be manufactured via sputtering and vacuum evaporation techniques [13].

All-solid-state thin-film rocking chair lithium batteries have been fabricated by means of sequential thin-film deposition techniques on flexible $80\mu\text{m}$ thick aluminum foil substrates. Their cell configuration was $\text{V}_2\text{O}_5/\text{Lipon}/\text{Li}_8\text{V}_2\text{O}_5$. The total thickness of the device did not exceed $1.41\mu\text{m}$. Such galvanic cells comprised thin-film electrodes of highly lithiated vanadium (V) oxide as the anode and vanadium (V) oxide as the cathode. By controlling the lithium concentration in the anode, one obtained an operating voltage in the range from

1 to 3 V. These cells had an active area of 15 cm^2 , and delivered a discharge capacity of $50 \text{ }\mu\text{Ah}$, at room temperature. Additionally, they showed negligible capacity fade from the second cycle to over 5800 cycles, at the current density of $10 \text{ }\mu\text{A}/\text{cm}^2$ [23].

Bates and co-workers fabricated and characterized thin-film rechargeable batteries equipped with an anode of metallic lithium and a cathode, which consisted of a mixture of amorphous V_2O_5 , crystalline and amorphous $\text{Li}_x\text{Mn}_2\text{O}_4$ [24]. These thin-film batteries operate with an amorphous inorganic electrolyte, which consists of amorphous lithium phosphorus oxynitride, known as Lipon. This electrolyte is typically deposited by RF magnetron sputtering [14]. The performance of the thin-film cells was evaluated at different current densities, at several temperatures. Electrical measurements showed that the current density of the thin-film cells was limited by the mobility of the Li^+ ions in the cathode materials. The internal resistance of the $\text{Li}/\text{Li}_x\text{Mn}_2\text{O}_4$ cells with crystalline cathodes was about two orders of magnitude lower than that of $\text{Li}/\text{V}_2\text{O}_5$ cells with amorphous cathodes [24].

Sequential thin-film deposition techniques enabled for the manufacturing of all-solid-state rechargeable thin-film batteries with the $\text{Li}/\text{Lipon}/\text{LiMn}_2\text{O}_4$ cell configuration. When cycled at room-temperature, these cells delivered the nearly constant voltage of 4.0 V at open circuit, good Coulombic efficiency, and the capability of carrying high current density. Planar microbatteries have been connected in series via metallization. For example, eight unit cells in series can deliver high voltage values up to ca. 32 V [25].

1.3.2 Flexible Zinc-Carbon Batteries

Circuit interconnects and various passive components can be fabricated on a variety of flexible substrates, by using the offset lithographic process. This approach enables for the manufacturing of Leclanch-type galvanic cells. In order to accomplish this task, it was necessary to develop zinc and carbon-based inks with appropriate rheological properties for lithographic printing. Zinc and carbon electrodes were fabricated with silver-based current collectors, and then, a separator material soaked in electrolyte has been in between zinc-carbon electrode structures and MnO_2 paste to form a galvanic cell [26].

Use of a combination of functional nanostructured materials allowed for the fabrication of optimum performance solid-state and flexible zinc-carbon batteries. Flexible carbon

nanofiber mats were obtained by electrospinning and utilized as the current collector and the cathode support. The cathode layer consisted of Mn(IV) oxide particles, which were mixed with single-walled carbon nanotubes (SWCN) for improved conductivity. A thin zinc foil served as the anode, while the electrolyte layer and a polyethylene oxide layer containing titanium oxide nanoparticles completed the system. This battery retained its performance even under mechanically stressed conditions, and its shelf-life was good [27].

A novel zinc ion conducting polymer gel electrolytes (PGEs) was made with non-volatile room temperature ionic liquids. PGEs consisted of an ionic liquid with a zinc salt dissolved in it, blended with a polymer matrix, poly (vinylidene fluoride-co-hexafluoropropylene), PVDF-HFP. Thus, one obtained electrolyte membranes, which were freestanding, translucent, flexible, and elastic; also, they exhibited excellent mechanical integrity and strength, possessed exceptional thermal stability, and did not show weight loss under dynamic vacuum or upon heating to 200 °C. The gel phase was stable in a wide temperature range, with ionic conductivities on the order of $10^{-3}S/cm$ at room temperature, $10^{-4}S/cm$ at $-20^{\circ}C$, and $(3 \sim 5) \times 10^{-3}S/cm$ at $80^{\circ}C$.

Electrochemical tests demonstrated that zinc ions possess mobility in the membranes, while zinc metal is capable of dissolution into the membrane, and can redeposit from the membranes. The membranes are stable in a wide Electrochemical potential window. PGEs based on ionic liquids show promise for potential application in next-generation non-aqueous zinc battery systems [28]. Recently, binary room temperature molten electrolytes based on acetamide and zinc perchlorate have been prepared and characterized. These electrolytes showed high conductivity at ambient conditions, and had favorable physicochemical and Electrochemical characteristics. Raman and infrared spectroscopic studies revealed the presence of large free-ion concentration in the molten liquid. Rechargeable zinc batteries assembled with a gamma-MnO₂ cathode, a metallic Zn anode, and operated with the molten electrolyte showed high discharge capacity over several cycles. It is expected that this class of acetamide-based, room temperature molten liquids should become a viable green alternative for electrolytes used in rechargeable zinc-based secondary batteries [29].

Room-temperature zinc ion-conducting molten electrolytes based on acetamide, urea, and zinc perchlorate or zinc triflate have been prepared and characterized by various physic-

ochemical, spectroscopic, and Electrochemical techniques. The ternary molten electrolytes are easy to make and can be handled under ambient conditions. They show excellent stability, high ionic conductivity, relatively low viscosity, and other favorable physicochemical and Electrochemical properties that make them good electrolytes for rechargeable zinc batteries. Specific conductivities of 3.4 and 0.5 mS cm⁻¹ at 25 °C are obtained for zinc perchlorate and zinc-triflate-containing melts, respectively. IR spectroscopy reveals that the free ion concentration is high in the optimized composition. Rechargeable Zn batteries have been assembled using the molten electrolytes, with gamma-MnO₂ as the positive electrode and Zn as the negative electrode. They show excellent Electrochemical characteristics with high discharge capacities. This study opens up the possibility of using acetamide-based molten electrolytes as alternate electrolytes in rechargeable zinc batteries [30].

A novel type of storage battery, which can be devised in various geometries, including nanoscopic and flexible systems, was built with microfabricated Zn/MnO₂ electrodes by using very special membranes, based on so-called "nanoglass" tubes. These tubes were developed in 2002 by Bell Labs and Lucent Technologies to provide a "super-hydrophobic nanostructured surface" atop of which a droplet of water or aqueous solution can be placed. Such a droplet would sit above the tubes, showing negligible interaction with the tubes. Inspiration came from smart surfaces found in nature, e.g., the surface of lotus leaves, which is not wetted by water. A honeycomb type silicon structure was manufactured by top down processing techniques, and this structure served as support for the battery, keeping the electrolyte physically separated from the electrodes until the battery was activated. [31]. It was demonstrated that upon applying an electrical voltage and current to the system, a droplet of liquid can be reversibly switched between the super-hydrophobic state or "rolling ball" state and the hydrophilic or immobile state [32, 33].

As a function of the applied voltage (as low as 22 V), liquid droplets on a nanostructured surface undergo sharp transitions between three possible wetting states, and liquid surface tension [34]. Under the action of an external voltage, the surface transitioned from superlyophobic to hydrophilic state. This phenomenon provides a novel means for manipulating liquids on the reduced micro scale [35]. By this the permeability of the entire structure can be tuned and such "smart" energy storage devices can be activated on demand. Upon

rigorously maintaining the spacing between the electrodes and the electrolyte, miniaturized reserve batteries can be obtained, which do not lose their power when not in use. This behavior is favorable, as over storage an average battery would typically lose as much as 7-10% of its power [31, 36].

One should emphasize here that the density of this cell that stays dormant over extended time periods enables the nanograss-based battery to serve as a so-called reserve battery or backup battery, traditionally used for special purposes, such as in emergency or military applications. [37]. “*Nanograss*” Zn/MnO₂ batteries provide an open circuit voltage of 1.55 V and a capacity of 200 $\mu\text{Ah cm}^{-2}$ [38].

A flexible galvanic cell and zinc-air battery were obtained by screen-printing on paper[39]. The galvanic cell consisted of a zinc/carbon/polymer composite anode, on one side of the sheet, and poly (3,4-ethylenedioxythiophene) (PEDOT) cathode, on the other side of the sheet. Lithium chloride and LiOH-based electrolyte was applied onto paper by inkjet printing, in between the two electrodes. This paper-based battery had an open-circuit voltage of ca. 1.2 V and a specific areal capacity of 0.5 mAh cm^{-2} [39].

1.3.3 Flexible Hybrid Power Sources

Comprising a thin-film organic or hybrid solar cell connected to a lithium-polymer battery, the so-called EURO-PSB device possesses attractive characteristics like low mass (below 10g), small thickness (less than 1mm), and mechanical flexibility. Owing to an efficient interconnection between the two devices, the battery is always charged with optimized voltage, independently of the illumination conditions. This product is compatible with roll-to-roll production processes[40] As pointed out in the Introduction to this chapter, various power storage devices, including hybrid systems and dual-storage battery-in-supercapacitor devices can be made with nonporous cellulose paper embedded with aligned carbon nanotubes [15].

1.3.4 Thin-Film Hydrated RuO₂ Electrodes

Electrodes based on hydrated ruthenium (IV) oxide are particularly relevant to the work disclosed in this Thesis. In all previously reported cases, however, RuO₂ has been utilized

as electrodes in supercapacitors, rather than in galvanic cells. Highlighted below are a few examples of such electrodes, including their preparation, analysis, and the system in which they are being employed.

Thin-film ruthenium oxide electrodes can be prepared by cathodic electrodeposition on a titanium substrate. Film thickness is being controlled by the deposition time. Such electrodes are used in supercapacitor applications, with 0.5M H₂SO₄ aqueous electrolyte. Morphological changes with increasing film thickness affect the specific capacitance and charge-discharge times of these supercapacitors. Maximum specific capacitance of 788F/g was achieved with an electrode with 1.4mg/cm² RuO₂. These results are explained by considering [41].

An alternative technique employed for depositing ruthenium (IV) oxide thin-films for solid-state thin-film supercapacitors consisted in direct current reactive sputtering, performed at 400°C. (TFSC). The supercapacitor has a cell structure of RuO₂/Li_{2.94}P O_{2.37}N_{0.75} (Lipon)/RuO₂/Pt. Radio frequency, reactive sputtering deposition of a Li_{2.94}P O_{2.37}N_{0.75} electrolyte film is performed on the bottom RuO₂ film, at room temperature, for electrically separating the bottom and the top RuO₂ electrodes. Scanning electron microscopy (SEM) revealed that the RuO₂/Lipon/RuO₂ hetero-interfaces had no inter-diffusion problems. Since the electrolyte thin-film has low ionic mobility, the capacity and cycle performance of the cell are inferior to those of a bulk type of supercapacitor [42].

A SnO₂-RuO, composite (SnRuO) thin-film possesses unique Electrochemical properties for a battery-supercapacitor hybrid due to the fact that the SnRuO system shows battery and supercapacitor characteristics simultaneously. SnRuO thin-films were prepared via magnetron co-sputtering method. The SnRuO thin-film as the anode in a secondary battery demonstrated a first discharge capacity of 1.557mAh/cm²; the second discharge capacity was, however, only half (52%) of the first discharge capacity. The SnRuO thin-film exhibited a specific capacitance of 14mF/cm² over 1000 cycles. These results suggest that SnRuO thin-films can be utilized as both a thin-film supercapacitor and a thin-film battery [43].

Electrostatic spray deposition (ESD) enabled for the manufacturing of ruthenium (IV) oxide thin-film electrodes with an average specific capacitance of 650F/g and high rate

capability. This technique is a one-step process as compared to multistep sol-gel processes. In addition, ESD offers the features of low-temperature synthesis and allows for an easy control of surface morphology. While as-prepared hydrous ruthenium (IV) oxide thin-film was amorphous, the hydrous ruthenium oxide, $\text{RuO}_2 \cdot \text{H}_2\text{O}$, thin-film became crystalline after annealing at temperatures $> 200^\circ\text{C}$ [44].

Chapter 2

THE ELECTROCHEMISTRY OF GALVANIC CELLS

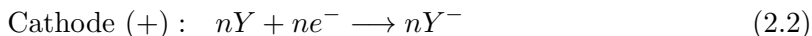
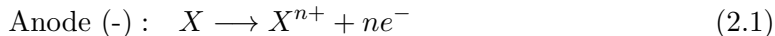
2.1 Brief description of battery operation

As stated in the previous chapter, one half of a battery is the electrolyte solution in contact with an electrode, called the *anode*, where the oxidation takes place. The other half-cell contains electrolyte in contact with another electrode, called the *cathode*, where the reduction proceeds [45]. Other essential components of a battery are the separator, current collectors, and packaging. In order to minimize the internal resistance of a battery the electrodes should be as close to each other as possible. The separator should be porous and thin. The separator is an insulating material, which prevents electrodes from touching each other, and, as a result, shorting the battery [46]. For open assembly of a battery in a container there is no need for a separator; the electrodes are immersed in the “*sea*” of electrolyte, and they will not touch each other. In case of a packaged battery, the pores of the separator will be impregnated with electrolyte, and the ions transfer through these pores.

At both electrodes chemical reactions take place, and generate electricity. Each electrode contains chemicals that participate in the reaction, and they are called *active materials*. The driving force for the external current derived from a cell is the difference in the electrode potentials of the two half-cell reactions [46]. Let us examine the chemistry that drives the galvanic cells.

The chemical reaction at the negative side releases electrons, and these electrons are

accepted by the current-collector of the positive electrode via the external circuit, when the battery is connected to a load. This electron transfer is complemented by the migration of ions in the internal circuit. Simplified reactions at the negative electrode and the positive electrode are illustrated below by equations (2.1) and (2.2), respectively:



During discharge of a battery, negative ions move toward the negative electrode, and positive ions move toward the positive electrode. The flow of these ions is reversed during the charging process [46].

2.2 Thermodynamic Considerations

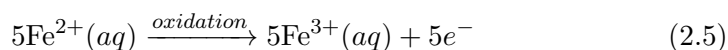
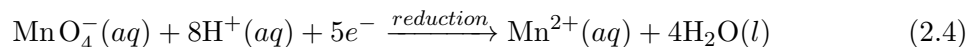
Galvanic cells generally operate close to thermodynamic equilibrium; hence, the “*ideal*” cell potential (standard cell voltages) can be predicted from thermodynamics. But most cells are not ideal. Thermodynamic analysis alone cannot tell us anything about the details of charge transfer (a non-equilibrium process), the over-potential (defined as the departure of cell potentials from thermodynamically determined standard potentials), or indicate what reaction(s) will proceed, and at what rate [47]. In the sub-sections below, I address some of these “*real-world*” chemistry issues.

2.2.1 Oxidation-Reduction Reactions

Oxidation-reduction reactions are chemical processes that involve transfer of electrons from a reducing agent to an oxidizing agent. In these reactions the reducing agent loses electrons, while the oxidizing agent gains those electrons. Below is an example of an oxidation-reduction reaction between Fe^{2+} and MnO_4^{-} , in acid solution, which proceeds according to equation (2.3):



Where Fe^{2+} is oxidized and MnO_4^{-} is getting reduced. The above reaction can be broken down into two half reactions, described by Equations (2.4) and (2.5):



As can be seen from the (2.3), electrons transfer directly from the reducing agent Fe^{+2} to the oxidizing agent MnO_4^{-} . This is, however, a chemical reaction, which does not generate current. When both the reducing agent and the oxidizing agent are in the same solution, electron transfer will happen directly, from one reactant to the other, in the solution, and no useful work is obtained.

In order for current to flow, the reducing agent and the oxidizing agent should be physically separated; this means that each half reaction should take place at a different electrode, and the electrons should transfer through a load connected to the electrodes by external wires. Hence, the key requirements for converting a redox system into an electrochemical system are (i) the physical separation of the reducing agent from the oxidizing agent, (ii) each electron exchange should occur at a different electrode, and (iii) the transfer of electrons should happen through an external loop, i.e., over an infinitely long pathway, as compared to the atomic scale, characteristic to redox reactions [48]. The result current can then power a load.

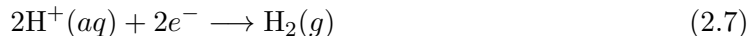
2.2.2 Electrochemical Potential

As discussed in the previous section, in a galvanic cell reduction and oxidation processes occur simultaneously. Each half-reaction has a potential associated with it. When we design a galvanic cell from a given pair of half reactions, the sum of electrochemical potentials of the

half-cell reactions determines the voltage of the battery. Standard reduction potentials for half-reactions are listed relative to the standard hydrogen electrode (SHE). By convention the reduction potential of a SHE is $0.000V$. For example, in a galvanic cell with zinc as the anode and SHE as the cathode, the potential of Zn is $+0.76V$, which is the standard reduction potential for zinc. In this cell, the anode is zinc metal in contact with Zn^{2+} solution. The oxidation half-reaction is, according to Equation (2.6):



On the cathode side, i.e., at the SHE, the reduction of protons takes place, as shown in equation (2.7):



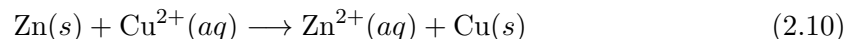
The overall cell reaction can be written as equation (2.8):



By definition, the voltage of this cell is equal to the standard reduction potential of zinc, as shown in equation (2.9):

$$E_{cell}^{\circ} = E^{\circ}(Zn^{2+}/Zn) - E^{\circ}(H^{+}/H_2) = 0.76V + 0.00V = 0.76V(\text{vs. SHE}) \quad (2.9)$$

Another representative example, known as Daniell's cell, consists of a combination of a zinc anode and a copper cathode, each in contact with its own ions. The overall cell reaction can be written as equation (2.10):



The standard voltage of a Daniell's cell is calculated from equation (2.11):

$$E_{cell}^{\circ} = E^{\circ}(\text{Zn}^{2+}/\text{Zn}) - E^{\circ}(\text{Cu}^{2+}/\text{Cu}) = 0.76V - (-0.34)V = 1.10V \quad (2.11)$$

Similarly, for any given cathode and anode pair the standard cell voltage can be calculated from tabulated standard potential values [49].

Thermodynamics provides an answer to the fundamental question of how one assigns a magnitude to the ideal cell voltage. But there are other questions that must be answered. We would like to know what combination of anode and cathode will or will not be able to perform work (i.e., to generate electrical energy.) We would also like to know the magnitude of currents that can be drawn from a particular cell. These quantities are limited by the chemical kinetics of the system. The rate of Electrochemical reactions is related to and measured in terms of current densities. In the next section we will examine the parameters, which affect and determine the magnitude of the current that can be delivered by a galvanic cell.

2.3 Kinetics of a Battery

We should define a series of electrochemical parameters involved in our discussion. First, the overpotential will be addressed, and next the voltage of a cell will be examined, as a sum of standard potentials, overpotentials, the Ohmic potential drop, and polarization losses.

2.3.1 Overpotential

The overpotential is an electrochemical parameter, which refers to the potential (voltage) difference between a half-reaction's thermodynamically determined reduction potential and the potential at which the redox event is experimentally observed [45]. The term is directly

related to a cell's voltage efficiency. Driving a reaction in an electrolytic cell requires more energy than thermodynamically expected. This excess of energy is quantitatively measured by the overpotential. In other words, no reactions can proceed in a system, while it is at equilibrium. In order to make the charge transfer reactions happen, one has to move out the system from its equilibrium state.

The overpotential is the extent to which the system is being pushed out from equilibrium. When a galvanic cell is discharged, less energy is recovered than thermodynamics predicts. This can be explained by asserting the existence of overpotential. Upon re⁻charging the cell, more energy is needed than predicted by thermodynamics, which means that the cathode and anode overpotentials will add to the charging voltage. In each case the extra or missing energy is lost as heat. Overpotential is specific to each cell design, and will vary between cells and operational conditions even for the same reaction. But when the cell is connected to a load, i.e., current is drawn from the system, and then the cell voltage will not be at its maximum value anymore [45, 50].

Equation (2.12) is the Tafel relationship between the overpotential, η , and the log of current density, $\log i$, flowing through the system; a and b are empirical constants [51].

$$\eta = a + b \log i \tag{2.12}$$

This empirical equation tells us how much one must change the potential (i.e., the magnitude of overpotential) in order to accomplish a certain current density [51]. This can also be written as equation (2.13):

$$i = A \cdot e^{\frac{B\eta}{RT}} \tag{2.13}$$

Where A and B are different from a and b , as one switches from 10-base logarithm to natural logarithm, and generalizes the relationship to any temperature (rather than 298K room temperature in equation (2.12)).

While Tafel discovered his relationship empirically, later it was derived on a theoretical basis, as a limiting form of the Butler-Volmer equation, equation (2.14), which predicts the net current flowing through the system

$$i = i_0 \left[e^{\alpha n F \eta / RT} - e^{(1-\alpha) n F \eta / RT} \right] \quad (2.14)$$

Where i_0 is the exchange current density, α is the electron transfer coefficient, n is the number of electrons involved in the Faradaic charge transfer process, T is absolute temperature, and F is Faraday's constant [52]. At extreme overpotentials the rate of one of the reactions, and, consequently, one term of the Butler-Volmer equation becomes negligible. Thus, when the positive polarization of the electrode exceeds $+120mV/n$ relative to the equilibrium only the oxidation reaction will proceed (according to (2.4)), the reduction being insignificant. By contrast, at negative polarization values of $\eta < -120mV/n$, reduction will take place, and no oxidation allowed. equation (2.15), which applies for anodic polarization, can be linearized as (2.16).

$$i = i_0 e^{1-\alpha} n F \eta / RT \quad (2.15)$$

$$\ln i = \ln i_0 + (1 - \alpha) n F \eta / RT \quad (2.16)$$

When converted to 10-base logarithm, and rearranged, (2.16) yields to (2.17), which is equivalent to the empirical Tafel relationship (2.12):

$$\eta = - [2.3RT / (1 - \alpha) n F] \log i_0 + [2.3RT / (1 - \alpha) n F] \log i \quad (2.17)$$

Hence, the physical meaning of the empirical constants a and b in (2.1) can be understood from the theoretical treatment, equations (2.16), as equations.(2.18) and (2.19) [50]:

$$a = -[2.3RT/(1 - \alpha)nF] \log i_0 \quad (2.18)$$

$$b = 2.3RT/(1 - \alpha)nF \quad (2.19)$$

Constant b , termed as the Tafel slope, provides information about the reaction mechanism, while constant a mainly reflects the rate constant of the reaction. Rigorously, Equation 1 should be written by using the absolute value of the current density, as shown in equation (2.20):

$$\eta = a \pm b \log |i| \quad (2.20)$$

Where the plus sign stands for the anodic overpotential, while the minus sign is used for the cathodic overpotential [50].

It should be noted here that the Ohmic resistance of the solution may cause deviations from the ideal electrode response described by equation (2.14). Therefore, in the real case one should amend the overpotential in equation (2.21) with a term, which accounts for solution resistance, R_s , the density of current flowing through the cell, i , and the exposed surface area of the working electrode, S , as shown in equation (2.21) [53, 54, 55]:

$$\eta = E - E^\circ - R_s IS \quad (2.21)$$

Use of Tafel plots, as an analytical tool for evaluating fuel cell performance has become popular over the past years; however, most studies are restricted to chemical power sources, rather than being extended to microbial fuel cells. Most likely, authors choose Tafel plots as their electroanalytical technique for uncomplicated electroactive processes, which have a well-defined stoichiometry. For such simple charge transfer reactions one can exploit the linear portion of the Tafel plot for deriving the number of electrons transferred in the process and the exchange current density, i_0 (by extrapolating the linear portion of the plot

to $\eta = 0$). The latter reveals the ability of the system to produce current, when moved out from the state of equilibrium.

Steady-state Tafel plots enable assessment of the electrocatalytic activity of various electrodes used in methanol or hydrogen based fuel cells. Hence, Tafel plots provide insight into the reaction mechanism of methanol oxidation on carbon-supported binary and ternary alloys of Pt, Ru, and Sn catalysts. Furthermore, these plots reveal changes in the rate-determining step, and when recorded at different temperatures, they allow for comparing the activation energy of different catalyst [56]. Also, they can identify the composition of catalysts with the greatest activity in methanol oxidation [57, 58, 59, 60]. Also, this analysis tool can be used for the performance assessment of the anode and cathode during direct methanol fuel cell operating conditions [61].

Another widespread application of Tafel plots in chemical fuel cells is the monitoring of reaction kinetics of oxygen reduction. Recent examples of this evergreen topic addressed by means of Tafel plots are the investigation of O_2 reduction in subfreezing polymer electrolyte membrane (PEM) fuel cells [62], the study of oxygen discharge mechanism in concentrated alkaline solution on hydrophobic cathodes [63], and the long-term durability testing of H_2 -air proton exchange membrane fuel cells [64].

The voltage of a battery, measured while connected to a load, is lower than its open circuit voltage. This can be the result of the internal impedance of the battery, which is made of up of [46]:

- Polarization losses at the electrode.
- Ohmic losses at the cathode, anode, in the electrolyte, and across the separator.
- Contact resistance.

All these phenomena can cause an unwanted voltage drop. Creating a limitation in charge transfer between the two electrodes. This is an intrinsic property of the electrodes in contact with the electrolyte. Another reason for the drop is due to the slow diffusion of the ions across the separator. This phenomenon depends on the thickness and porosity of the electrodes as well as of the separator. Ideally, we want the voltage drop across the cell

should be minimal, when connected to the load. In order to achieve this goal, studies need to be done for reducing the polarization losses at the electrodes. Various compounds, such as manganese (IV) oxide, commonly referred to as manganese dioxide or ruthenium (IV) oxide can be used as depolarizer.

Overpotential losses are present both at the cathode side and the anode side, and manifest as both charging potential and discharging potential. The increased and decreased cell potential during charging and discharging can be calculated from equations (2.22) and (2.23) [46].

$$V_d = V_r - \eta_+ - \eta_- - IR \quad (2.22)$$

$$V_{ch} = V_r + \eta_+ + \eta_- + IR \quad (2.23)$$

Where V_d , V_{ch} , and V_r are discharge voltage, charge voltage, and reversible voltage or open-circuit voltage, respectively.

Ideally, we want to minimize the overpotentials (make them zero), so that the equation above can be written as:

$$V_d = V_r - IR \quad (2.24)$$

$$V_{ch} = V_r + IR \quad (2.25)$$

Since the ideal case is not achievable, we will not be able to reduce the over potential to zero. As mentioned earlier, a system with overpotential Zero is in equilibrium, hence it cannot perform work, and hence, it cannot generate electricity. We need, however, to reduce as much as possible all unnecessary overpotentials in our cell, e.g., by using different kinds of depolarizer or employing more porous and thinner separators.

2.4 Chemical and Physical Considerations of a Galvanic Cell

2.4.1 Electrolyte Effects

The electrons exchanged in the chemical processes that drive a galvanic cell are carried across the internal circuit, i.e., by the electrolyte, via the directional stream of oppositely charged ions [51]. Hence, ions act as charge carriers in the internal circuit; once they reach the electrodes, they may undergo electrochemical processes or, alternatively, other species may discharge at the electrodes, and account for the charge transfer in the internal circuit of the cell. In order to achieve highest efficiency, the electrolyte must contain high concentrations of the ions. On their turn, ions should exhibit high mobility. Owing to its high polarity (with a dipole moment of 1.85 debye), water is a favorable solvent of inorganic and organic salts, contained in the electrolytes [51]. Pure water undergoes ionization to a very limited extent (2.26):



Where the concentrations of $[\text{H}^+] = [\text{OH}^-] = 10^{-7} \text{mol}/\text{cm}^3$ (at 20°C). Such low ion concentrations do not allow the current to be transported through pure water, which is an insulator (specific resistivity of de-ionized water is $18.2 \text{M}\Omega\text{cm}$, at 25°C). Consequently, water can be used as an electrolyte only after a “supply of ions” has been added in it, i.e., an acid, a base, or a salt has been dissolved in it.

Electrolytes for Zn – RuO_x cells can be made in an alternative manner. They are not necessarily aqueous solutions, but hydrogels with incorporated ions can also be used as the electrolyte. Such solid electrolytes exhibit advantages over liquid ones, owing to their ability of preventing battery dry out and leakage.

Fundamentals

As stated previously, batteries consist of two electrodes, which are electronic conductors, separated by an electrolyte solution or gel, which is an ionic conductor. The latter plays the role of closing the internal circuit of the cell. Several features need to be considered for choosing an electrolyte for a system. Below is a list of such parameters:

- The electrolyte should be compatible with the system. It should not be too acidic or excessively alkaline as to dissolve the electrode (or separator) materials. On the other hand, close to neutral electrolytes have proven Electro chemically inactive. Depending on the type of the electrodes, the electrolyte should be chosen to contain sufficient concentration of ions for transporting an ion current equivalent to the electron current streaming through the external circuit.
- Electrolyte should be chemically stable, i.e., it should not decompose over time and its pH should be constant.
- Electrolyte should be electro chemically stable, which means that it should exhibit a potential window compatible with the operation voltage of the galvanic cell.
- High conductivity represents a major requirement of a good electrolyte, so the ions can transfer without being hindered. High conductivity of the electrolyte will reduce the overall internal resistance of the cell and, consequently, the Ohmic potential drop, which may cause significant losses in efficiency of the galvanic cell (the cell voltage of the battery would be decreased). We attempt to lower the internal resistance of a battery as much as possible.
- As we are concerned about the safety, the electrolyte should not to be flammable, which applies for most electrolytes based on organic solvents. Also, it should be environmentally friendly and nontoxic.
- The effect of the pH of the electrolyte appears to be a complex phenomenon. Different pH values may cause different results in battery performance and cyclability. Depending on the type of electrodes and their purity, the separator material and its

thickness, as well as the form factor of the galvanic cell as a, electrolytes of different pH value will perform differently.

Concepts of Electrolyte Conductivity

The ability of an electrolyte solution to sustain the channel of electrical current depends on the mobility of its ions, driven by the electric field between electrodes [65]. If ions of charge Z_{e_0} are accelerated by the electric field strength, E , and are subject to the Stokes frictional (or viscous) force, F , which increases with the drift velocity v_d , and is given for simple spherical ions of radius r_i , then the frictional force can be calculated by equation (2.27), where η is the viscosity of the medium [65].

$$F = 6\pi\eta r_i v_d \quad (2.27)$$

The absolute mobility of ions, u_{abs} , is defined for diffusing particles by dividing the drift velocity by either the diffusional driving force or the equal and opposite Stokes viscous force, equation (2.28) [65]:

$$u_{abs} = v_d / 6\pi\eta r_i = 1 / 6\pi\eta r_i \quad (2.28)$$

In the electrochemical literature ion mobility is typically expressed as conventional (electro chemical) mobility, u_{conv} , which represents the drift velocity in unit electric field ($1V/cm$). The relationship between absolute and conventional mobility is given by equation (2.29):

$$u_{conv} = u_{abs} Z_{e_0} \quad (2.29)$$

When the velocity attains a limiting value V_{max} corresponding to the exact balance between the electrical and frictional forces, equation (2.30) applies:

$$Z_{e_0}|E| = 6\pi\eta r_i v_d \quad (2.30)$$

For a given values of η and $|E|$, each type of ion will exhibit a transport velocity, v_d , dependent on the charge and the radius of the solvated ion, and a direction of migration, which is determined by the sign of the charge [65].

$$u_{conv} = Z_{e_0}/6\pi\eta r_i \quad (2.31)$$

The ion of greatest mobility is H^+ , therefore, its presence in the supporting electrolyte will enhance the overall conductivity. In our system, acidic electrolytes have proven efficient. However, the pH value of the solution (or gel) should represent a trade-off between high electrochemical activity in the galvanic cell and moderate chemical activity, when the cell is not in use, so that the unwanted chemical corrosion of zinc anodes can be avoided, and the shelf life of the battery increased.

Conductivity

Conductivity, just like the resistivity, is a characteristic property of the material, and does not depend on the geometric factors. We seek to define the conductivity for a given electrolyte solution, which will be characteristic of the solution, and independent of geometrical factors. For a cell with a uniform cross-section A , while the two electrodes are separated by a distance d , and has the conductance L , then the conductivity K_1 can be calculated from equation (2.32) [65]:

$$K_1 = d \cdot L/A \quad (2.32)$$

Conductivity is measured in units of $\Omega^{-1}m^{-1}$ or Sm^{-1} .

2.4.2 Separators

Battery separators provide a barrier between the anode and the cathode. The separator physically separates and electrically insulates the anode from the cathode but it allows electrolytic or ionic conduction to occur through the electrolyte [66]. Hence, the battery separator must be a good electronic insulator, Electro chemically stable in the presence of the electrolyte and electrode materials, and it must be ionically conductive [67].

The major parameters that affect the performance of a separator in a battery are:

- Electrical resistance which can be calculated with Ohm's law
- Porosity
- Water absorption
- Electrolyte absorption and retention as needed by the ion transport.
- Dimensional stability, meaning that the separator should stay flat and not curl at the edges.
- The separator should not swell or shrink during electrolyte absorption.
- Chemical stability over a long time period meaning that the separator should be able to tolerate the strongly oxidizing cathode and the corrosive electrolyte at high temperatures.
- Thickness and uniformity of properties. For flexible thin-film batteries, a thin separator is needed to maintain the form factor.

The electrical resistance of the separator is the most important factor. The goal is to pick a separator that has the smallest internal resistance while having the smallest thickness. There is a trade-off between the thickness and the capacity of the cell when it comes to the separator. Analysis in section 5.3 shows the effect of different separators and their thickness on the total capacity and performance of the battery. Most likely, having a thicker and more porous separator will give a better result because more electrolyte can be absorbed by the separator. This will help the battery to have longer life time. The internal resistance of

the cell can be calculated by Ohm's law. subsection 4.2.5 explains in more detail how the internal resistance of a cell can be calculated. To summarize, the internal resistance is the cause of the extra voltage drop of the cell, when connected to the load. Table 5.4 shows the internal resistance of the cells with different separator materials.

Chapter 3

FABRICATION AND CHARACTERIZATION OF NOVEL ZINC-RUTHENIUM OXIDE CELLS

Let us now turn to the details of the ruthenium oxide/zinc cells that form the basis of this Thesis. We address each of the separate components of the battery sequentially.

3.1 Chemical Considerations for Novel Zinc-Ruthenium Oxide Cell

This section of this Thesis deals with the chemical consideration of Zn- ruthenium oxide cell. It looks closely at the cathode side and the anode side and their effects on the performance of a battery. It also looks into the effects of electrolyte on the battery operation.

3.1.1 Close Look at the Cathode Side

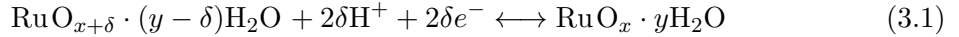
Ruthenium oxide has been used in recent research to achieve high value capacitances. It has the highest capacitive storage of any known material in the world ($\sim 1400F/g$), and has been the subject of many papers [68]. Ruthenium oxide is non-toxic and environmentally friendly. It can also be found abundantly in the planet. Initially, ruthenium dioxide was used for super capacitors, but due to the materials cost and internal leakage current, its market is very limited now. However, ruthenium dioxide does not have these disadvantages, when used in batteries. The proposed battery in this study shows that none of these shortcomings have been observed when using RuO_2 as the cathode material. In the proposed battery, oxidation-reduction takes place at a metallic anode, such as a zinc or aluminum. The choice

depends on the desired output voltage.

RuO_x films can be produced Electro chemically or thermochemically. Electro chemically formed RuO_x films are often hydrous, and thus, are open to much easier proton transfer through the lattice. These hydrous films exhibit a great component of pseudocapacitance, as compared to a much smaller component of double-layer capacitance. The conductivity of RuO_2 allows for easy electron transfer from the surroundings, and is facilitated by H^+ transfer from an electrolyte. Therefore, RuO_2 electrodes can be charged/discharged by a coupled electron/proton transfer process.

Ruthenium has many oxidation states, range from 0 to +8, and -2 . The +2 and +3 and +4 states are the most common stages [69]. Most reversible redox reactions are observed between the states +4 and +2. In surface regions of RuO_x films, oxidation states between +2 and +6 can be assessed. There is some support for the belief that reaction, yielding for Ru oxidation states greater than +6, especially at high potentials, may not be reversible [69].

For hydrated ruthenium oxide, the following type of redox reaction occurs between states +2 and +4 equation (3.1):

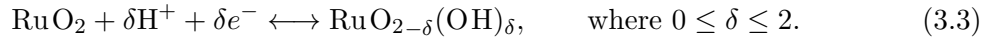


In this reaction, the left-to-right direction involves the reduction of ruthenium oxide. For instance, take $x = 2$ and $\delta = 1$. On the left-hand side, the hydrated RuO_x specimen is Ru_2O_3 , with the ruthenium at the oxidation state of +3. In order to be converted to RuO_2 on the right-hand side, the ruthenium gives up one oxygen to form one more molecule of water of hydration with two extra hydrogen ions, which should be available in the medium (e.g. from an acidic electrolyte). In the process, the oxygen atom is being released from the ruthenium oxide, and requires two additional electrons and two protons to form the covalent bonds $\text{H}^-\text{O} - \text{H}$, i.e., the “*new*” hydration water molecule. These electrons should be supplied from an external circuit, while the supporting electrolyte contained by the cell supplies the necessary H^+ ions.

It has been suggested that in some fraction of available surface states, the reaction shown in equation (3.2) takes place:



With $x = 2$ and $y = 0$, this reaction becomes, equation (3.3):



The above proton-assisted reduction processes of ruthenium oxides were investigated by cyclic voltammetry, abbreviated as CV. section 5.5 looks into cyclic voltammetry experiments in more detail.

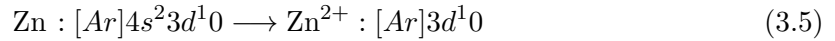
The discharge of a RuO_2 cell shows a number of plateaus, indicating the participation of a number of valence states. Let us assume that the entire mass of the RuO_x nanosphere was hydrated in the discharge reaction. According to Conway, the hydration reaction may extend into the bulk. Our particles may be small enough to assure complete hydration of the material mass. We can derive an expression (based on density, molecular weight, and an assumed number of participating electrons) for the mass of the oxide (M) required for achieving the observed capacity, equation (3.4):

$$M = 2.5C_p \quad (3.4)$$

Where M is in mg and C_p is in mAh/cm^2 . We have assumed that each Ru(IV) oxide unit contributes 2 electrons. Thus, to achieve a capacity of $5mAh/cm^2$, we would need $12.5mg$ of the oxide. As the density of the oxide is $7.14g/cm^3$, we would need a thickness of $17.8\mu m$. The amount of the ruthenium used in one cell is normally more than above, therefore we expect to get more capacity per area. Some of the cells provide up to $10mAh/cm^2$ before dry out.

3.1.2 Close Look at the Anode Side

The reaction on the zinc side is relatively simple. Below is the oxidation reaction at the zinc side, equation (3.5),(3.6). Considering the electron configuration of zinc, it can be noted that zinc has two free electrons in the outer shell and during the oxidation it loses these two electrons becoming Zn^{2+} :



The reaction on the zinc side is however pretty simple.



As described in chapter 2, the standard electrochemical potential of zinc is $0.76V$ and the electrochemical potential of the ruthenium is $0.45V$. As a result, the overall potential of the cell is around $1.2V$. Depending on the electrolyte the potential may vary by $\pm 0.2V$. One finds the following relationship for capacity (in mAh/cm^2) as a function of zinc foil thickness and surface area of the cell:

$$d = 1.74C_p/A \quad (3.7)$$

Where d is the thickness in microns, C_p is the capacity (mAh/cm^2), and A is the projected geometric surface area of the cell. Using equation (3.7), we can calculate the thickness needed for a cell. For example, for getting $5mAh/cm^2$ of capacity, we would need thickness of the zinc equal to $8.7\mu m$ for a $1cm^2$ cell. A commercially available $25\mu m$ zinc sheet will more than suffice for each $10mAh$ of capacity, with sufficient safety margin to prevent etch-through and the development of a non-recharging surface.

Different zinc thicknesses are used to make our novel battery. The goal is to reduce the

thickness of the zinc electrode as much as possible. Zinc foils as thin as 0.001” or 0.003” can be used in battery manufacturing.

3.1.3 Close Look at the Cell Capacity

The general method used to experimentally determine the charge capacity of a cell is to run it across a constant load by using potentiostat. Many attempts have been made to increase the capacity of a cell. One fundamental technique of changing the capacity is to use different electrolytes. In an effort to obtain the greatest capacity value, we have tested a variety of electrolyte compositions. Figure 3.1 is an example of constant load discharge of a 4cm^2 cell through $1\text{k}\Omega$ load. Close look at the curves shows a very fast drop of the potential, which indicates the magnitude of internal resistance. Then, in 6h into the discharge, we see a very rapid drop-off in voltage. Next, we observe a plateau lasting out to 14h , where the voltage drops to 0.5V . A secondary plateau along with a long tail follows this.

We interpreted these results as follows. Through a reduction process at the cathode side, the cathode assembly starts hydrating and going through its possible valence states. As the RuO_2 is reaching a saturating level of hydration, we theorize that electrons (derived from the anode) continue to be injected into the electrolyte, discharging hydronium ions, i.e. H_3O^+ , and electrolyzing water, as well, and that this creates the secondary plateau. Further, atomic hydrogen, created by the previous processes and stored as an adsorbate on the surface of activated carbon (henceforth: AC) particles, may yields molecular hydrogen, subsequently coalescing to form bubbles, which can increase the series resistance of the battery, and cause the decline of the output voltage across the load.

3.1.4 Initial Electrolyte Utilized in $\text{Zn} - \text{RuO}_x$ Galvanic Cells

The initial cell was implemented with an electrolyte composed of a weak acid and ethylene glycol, with ammonium hydroxide blended in the ethylene glycol. This mixture had a close to neutral pH value, and prevented rapid dissolution of both the electrode materials and the package sealing materials, while providing the needed conductivity. However, the capacity drawn with this electrolyte was only 0.0325mAh/cm^2 . As part of the improvement of battery performance, various types of electrolytes with different compositions and different

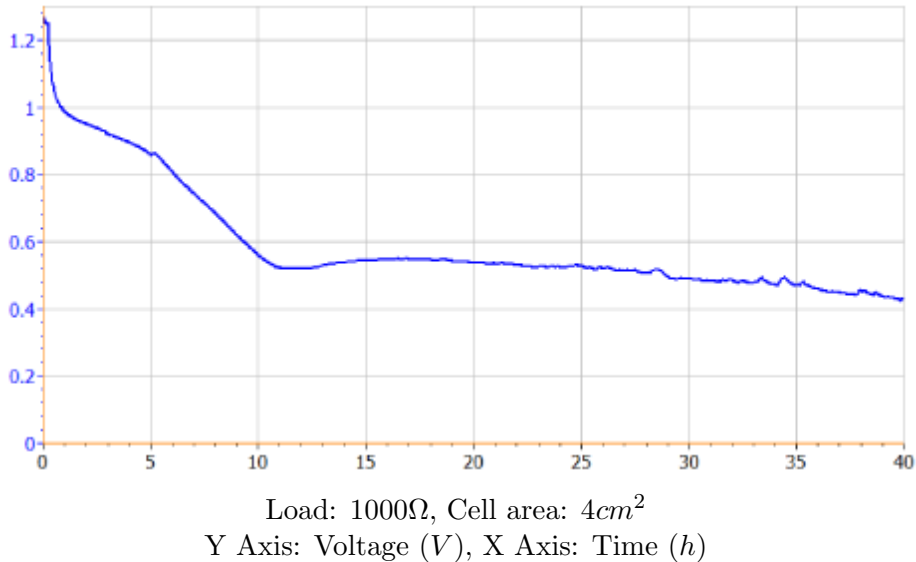


Fig. 3.1: Constant load discharge of a 4cm^2 cell through $1\text{k}\Omega$ load.

pH value were tested.

More recent research revealed that there are tradeoffs in increasing the conductivity of our electrolyte, as follows: (i) Although, high ion concentration will augment the conductivity, it will also cause faster dry out in the cell. This degrades the shelf life of the galvanic cell. It appears that higher ion concentration implies more water molecules and are tied up hydrating the ions. As the hydration water is tightly attached to the cations and anions through dipole⁻charge interaction, less free water is available at the RuO_x -based anode for balancing the Faradaic process at the cathode; (ii) While high ion mobility of H^+ , in acidic electrolytes, or OH^- ions, in alkaline electrolytes confer favorable conductivity to the electrolyte, they also promote unwanted corrosion phenomena in the cell. Corrosion is detrimental to shelf life.

The use of a gel electrolyte can yield important advantages for ease-of-manufacturing and battery operational life, as well as in preventing the increase of internal resistance due to hydrogen evolution. Also, it may improve cycle life by reducing dendrite formation. Replacing the electrolyte solution by a thin gel, such that it maintains the performance of batteries equipped with a regular separator is a challenging task. Our goal is to make a gel electrolyte that provides the same charge capacity as aqueous electrolytes, while it prevents the dry-out of the cell. Some explorations have been conducted in the space of electrolyte

viscosity, and we have demonstrated the operation of batteries with an alkaline gel-based electrolyte. Further explorations and experiments are needed for a better understanding of the material composition of gels and thinning techniques for rendering their thickness appropriate for use in flexible batteries. The further study of gel electrolytes and their performance was beyond the scope of this Thesis.

3.2 Physical Consideration and Fabrication of a Novel RuO_2 Cell

In this section we overview the fabrication process for the battery. We implemented the cells with an electrolyte made of an acid and ethylene glycol. Different types of electrolyte have been used that will explain in subsection 5.1.2. The systems of the materials and the packaging have been chosen to yield a light, small volume, flexible and thin cells. $\text{RuO}_2 \cdot x\text{H}_2\text{O}$ (hydrated ruthenium oxide) was compounded with another material, and used in the battery as the cathode material. The compound forms a conducting paste that is added as a thin layer atop of a flexible substrate. Typically, we use graphite sheet as the backing for the cathode side. However, different types of current collectors have been tested to give the highest flexibility and conductivity. The electrolyte is added over the powder to make a slurry-like mixture. This layer is covered with a separator, and then an anode electrode will go over the separator. The cell will be packed in a thin plastic package, and sealed using its adhesive side. The edges of the plastic packaging will be sealed with heat or tape. Figure 3.2 shows the cross sectional view and the top view of the battery.

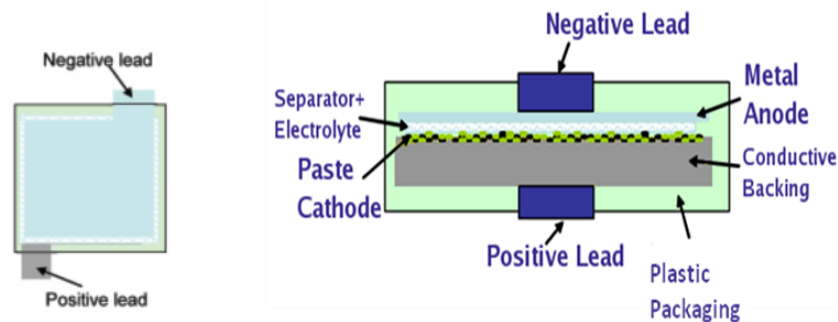


Fig. 3.2: (a)Top view of the battery. (b) Cross sectional view of battery.

The battery is rechargeable and flexible, so that flexible electronics may be integrated on it, which may be used for power distributed networks node devices. In summary, the cell includes: an anode, a cathode, an electrolyte, separator, and flexible packaging.

Varieties of these parts have been used to make the battery as thin as possible, while keeping its flexibility and high current capacity.

In fabricating a ruthenium oxide battery we should consider following factors to get the highest performance. Acetone and aqueous ammonia solution (3wt.%) are used to clean the surface of the anode, which is typically zinc foil. While acetone removes the organic impurities, such as grease or oil, ammonia solution etches slightly the surface of Zn. It dissolves and removes a very thin Zn layer from the electrode surface, and thus, exposes a fresh, active Zn layer to the electrolyte.

The separator needs to be cut slightly bigger than the active area of the cell so it prevents any accidental short-circuiting internal to the battery. Since drops of electrolyte will be added to the separator, caution needs to be taken not to add excessive amounts of electrolyte, which would leak through the battery. The added aqueous solution serves as the ionic conductor in the internal circuit of the cell. The entire volume of electrolyte should be accommodated by the galvanic cell, so that no leakage occurs.

The contacts on the electrodes should be large enough to prevent any current crowding. In other words, the contacts should be large enough, so that ions have enough space to migrate. Small contact will cause ions to cluster at the surface of the contact and increase the internal resistance of the battery. Internal resistance is an important to the performance of a battery. We attempt to make internal resistance of the battery as small as possible. So the voltage drop across the resistance will be smaller and this yields a better performance of the battery. Contacts are made to the electrodes with the aid of conductive epoxy (if necessary). Details about the internal resistance of a battery are explained in subsection 4.2.5. Finally, the battery needs to be sealed properly, for preventing any liquid evaporation that results in the premature death of the battery. Another important factor to keep in mind is that the existence of the contacts will not interfere with the voltage of a cell. The contacts are not in direct contact with the electrolyte so they don't interfere with the chemical reaction that takes place inside the cell.

3.2.1 Initial Separator Utilized in Zn – RuO_x Galvanic Cell

In the novel flexible battery we have used glass fiber separators designed for air sampling and other applications. These filter papers, such as Model FP810 by F&J Specialty Products, are made of 100%high quality borosilicate glass micro fibers, and contain less than 5% acrylic binder. Their thickness is $0.38mm$ and their dry tensile strength is $5lb$ per inch width. They are chemically inert in acidic or alkaline solutions, and are thermally stable at temperatures up to $500^{\circ}C$. These separators have high load capacity, meaning that they have the ability of collecting particles without clogging or cessation of flow.

3.2.2 Thin Separators

Our ultimate goal is to reduce the thickness of the cell by thinning different components of the cell. Given the relatively high thickness of the glass fiber separator, different commercial membranes available for Li-ion batteries were tested for thinning the overall cell. Battery separators manufactured by Celgard, LLC are highly-engineered and offer many options of varying thickness, porosity and Gurley number. Also, American Membrane Corporation provides a variety of separators with different pore size. The thickness of the separator is around $90\mu m$, with a variety of pore sizes spanning from $0.03\mu m$ to $10\mu m$. The results of battery performance of with different types of separator are summarized in section 5.3.

3.2.3 Cathode Current Collectors

A variety of cathode materials have been explored for their ability to collect electron charge, and provide a low resistance material, able to transfer electron current into the electrolytic medium [68]. Throughout this Thesis, the standards Zn – RuO_x batteries feature a $0.13mm$ thick graphite foil as the cathode current collector. The cathode side of the battery consists of ruthenium hydroxide mixed with activated carbon, in a paste. Two problems are encountered when using graphite foil in the system. The thickness of the graphite has a major impact on the overall thickness of the battery. Since the goal is to reduce the thickness as much as possible, one of our main concerns is to replace the graphite foil with thinner materials. Another weak point of using graphite foil is the experimental observation that

the material absorbs electrolyte, reducing the amount of available liquid inside the battery; this phenomenon contributes to the mechanical problem of dry-out noticed for our cells.

To overcome this problem, we have investigated alternative cathode materials, such as carbon-based mesh, carbon-based cloth, carbon-fiber veil, as well as carbon nanotube films, known as “*buckeye*”. We achieved relatively high capacity from these alternatives; however, the graphite foil is still our primary current collector, because of its low cost and easy handling. section 4.2 illustrates the performance of batteries and their internal resistance, when using each of these materials.

Since the current collector does not exert any effect on the chemistry of the cell, it should be as thin as possible, and should have very small internal resistance. One approach to identify such materials is to evaluate ultrathin fibers or similar materials, as the substrate coated with a thin layer of chemically insulating, electrically conductive polymers [68].

3.2.4 Anode Current Collectors

In a galvanic cell, the anode is the negative electrode from which electrons flow out to the external circuit. Since electrons move from the negative electrode to the positive electrode externally the current flows from the cathode towards the anode via a load.

Anodes are metals, which are corrodible in electrolyte that leads to reduction reaction inside the cell [70]. In the general case, the reaction on the anode side can be summarized as:



Where M represents the pure metal, while M^{2+} are its ions.

Metallic anodes have the advantage of a high electrical conductivity. This reduces the internal resistance of the cell on the anode side. There are two important criteria in choosing the anode materials. Weight and volume are the main factors for flexible battery systems. The parameters under consideration are the density of the materials, its energy density, and its equivalent weight relative to the released charge. Table 3.1 shows some examples of

these parameters for different anodic materials used in batteries [70].

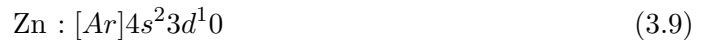
Aluminum and zinc are the common anode materials, which are used throughout this Thesis. The anode material is important in releasing a hydrogen atom in reduction reactions. Zinc is one good example of anode electrode that has been used in different types of batteries such as Ni – Zn, Zn-carbon and alkaline batteries.

Active Material	Mass Density (<i>g/mL</i>)	Equivalent weight (<i>g/charge</i>)	Energy density (<i>Ah/kg</i>)
Al	2.7	9	2980
Cd	8.7	56	480
Li	0.53	7	3830
Mg	1.7	12	2230
Na	0.97	23	1170
Zn	7.1	33	812

Tab. 3.1: The anodic material used in batteries.

3.2.5 Anode in Zn – RuO_x Galvanic Cell

Zinc is a main anode material used in the novel ruthenium cell. As described before, the reaction on the zinc side is pretty simple. Below is the oxidation reaction at the zinc side. Considering the electron configuration of zinc, it can be noted that zinc has two free electrons in the outer shell, and during the oxidation it loses them to become Zn²⁺ ion.



and when it loses the valence electrons it becomes:



The reaction on the zinc side is pretty simple, according to equation (3.11):



As described in chapter 2, the electrochemical standard potential for the $\text{Zn}^{2+}/0$ redox couple is $0.76V$, and the electrochemical potential of the ruthenium is $0.45V$ (at pH zero). As a result, the overall standard cell voltage is around $1.21V$. Depending on different pH values of the electrolytes, the potential may vary by $\pm 0.2V$.

Based on Faraday's law of electrolysis, one can derive the relationship in equation (3.12) for capacity (in mAh/cm^2) as a function of zinc foil thickness and projected geometric surface area of the anode in the cell:

$$d = 1.74C_p/A \quad (3.12)$$

Where d is the thickness of the Zn foil in microns, C_p is the capacity (mAh/cm^2), and A is the projected geometric surface area of the cell. Using the above equation we can calculate the thickness needed for a cell. For example, to get $5mAh/cm^2$ of capacity, we would need thickness of the zinc equal to $8.7\mu m$ for a $1cm^2$ cell. A commercially available $25\mu m$ zinc sheet will more than suffice for each $10mAh$ of capacity, with reasonable safety margin to prevent etch-through and the development of a non-recharging surface.

Different zinc foil thicknesses are used to make our novel battery. The goal is to reduce the thickness of the zinc electrode as much as possible. Zinc foils as thin as $0.025mm$ or $0.075mm$ are used in battery manufacturing. Since the cost of thin zinc foils is high for thin sheets, commercially available thicker zinc material will be used in battery testing; their thickness is $0.6mm$, and it is one order of magnitude cheaper.

There are some disadvantages associated with zinc-based systems, as listed below [68]:

- The materials form dendrites that cause the separator to become rigid or penetrate through the separator and short out the cells.
- Zinc surface changes shape during the charging and discharging processes. Zinc clumps

in one area and disappears in other areas. This causes current crowding and local heating and, as a result, malfunctions of the electrode.

- Formation of insoluble zinc oxides.

Adding ethylene glycol to the electrolyte provides help in solving the dendrite problem. However, we have not experienced any dendrite shorting, as the glass-fiber separator, which is very thick. We have observed a piece of filter paper under microscope, after the battery went through a discharge. Figure 5.15 shows this image. The black areas correspond to the ruthenium remaining on the filter paper, and the white and green areas represent the filter paper. As can be seen, there is no sign of dendrite formation on the filter.

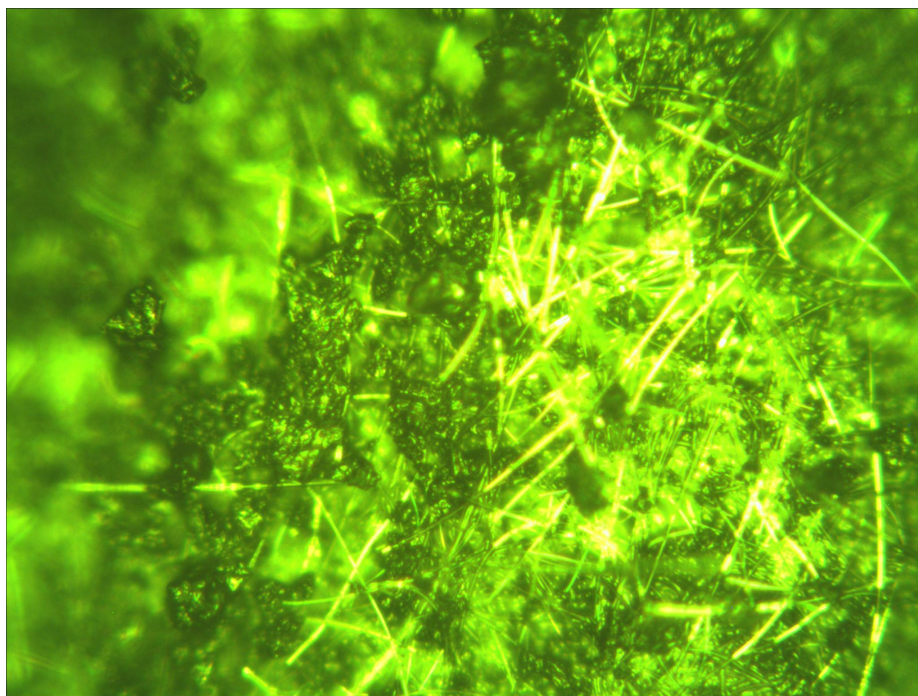


Fig. 3.3: Piece of a separator under the microscope.

Since using thick zinc allows for a considerable safety margin, the size effect issue is under control. However, utilizing thinner zinc with our current electrolyte sometimes results in eating through the zinc anode, and creating holes. Part of the ongoing effort is to determine the minimum zinc thickness required for successful cell operation. section 2.4.1 looks into different methods used to obtain thin zinc. It will also examine the performance of the battery obtained via these Zn “*thinning*” methods.

Adjusting the pH of the electrolyte eliminated the formation of insoluble zinc oxides. Initially the battery was made by using pH 5 electrolyte. Changing the pH to more acidic values helped in solving this problem. subsection 5.1.2 analyzes the effect of electrolytes with different pH and their chemistry on the battery.

Other Anode Materials

In addition to zinc, which has been so far the default anode material for our novel ruthenium oxide batteries, it is possible to explore other anode materials. A possible candidate is aluminum, a main group metal. Aluminum has been used as an anode material owing to its low price, light weight, and also its availability in different thicknesses. Considering the electron configuration of aluminum, shown below, equation (3.13), it can be observed that it has three electrons in its outer shell; these are the valence electrons that are involved in the oxidation reaction of Al.



Consequently, according to equation (3.14) the reaction on the aluminum side will be:



The standard reduction potential of aluminum is $-1.662V$ [71], and since the electrochemical standard potential of ruthenium (IV) oxide is $+1.120V$ [71], the total cell voltage is expected to be $2.782V$. The practical value of the cell voltage of the Al – RuO_x battery will, however, not exceed $1.4V$, as the battery is not operated under standard pressure and temperature ($1atm$ and $298.15K$), and the electrolyte in contact with the electrodes is of different composition than that corresponding to standard conditions (H^+ concentration of $1mol/L$, i.e., $pH = 0$). Given that our electrolyte is mildly acidic (typical pH values in the range from $pH 2.5$ to 5.5), it may not remove the native Al₂O₃ layer from the aluminum

surface. This thin, highly adherent aluminum oxide layer prevents Al dissolution in many environments [72], which affects on one hand, the measured cell voltage (i. e., the thermodynamics of the process), on the other hand, it decreases the rate at which metallic aluminum can be oxidized (i. e., the kinetics of the process).

The advantage of aluminum over other metals is that cells equipped with Al anodes can be recharged at very low voltage. Envisioned applications are in devices that need to be recharged by harvesting various low power energy sources, such as RF energy or microwaves. It is mostly used in sensor application, where the battery should be charged remotely.

To summarize, Al is a good candidate for anode material, owing to its low cost and its light weight. However, aluminum is widely known to oxidize very fast and for this reason it is not our main option for the anode material.

Anode Optimization

As already described, our battery uses metallic zinc as the oxidizing half cell (anode). Zinc offers several advantages over other candidate metals, such as (i) exchange of two electrons per atom, (ii) Zn is available in chunks or plates at low cost. In ingot form, bulk zinc costs only about 0.3 cents per gram. Thin zinc foils are, however, expensive. Hence, anode cost is a significant component of the overall galvanic cell. In order to reduce the cost of the anode, we initiated avenues toward electroplating zinc onto thin metallic supports, including copper, aluminum, and stainless steel mesh.

Our thinnest prototypes to date use very thin foils of zinc (1 to 3 mils in thickness) for demonstrating energy density and flexibility. These foils are manufactured with much higher tolerances than our galvanic cells require, and involve labor intensive processing, which makes them far more expensive than is necessary for use in a battery. At present, they are the highest cost battery component, despite being the lowest cost raw material in the battery. Thus, one of the objectives is to develop a low cost method for producing a $50\mu\text{m}$ to $100\mu\text{m}$ thick zinc anode.

This process involves three stages: (i) degreasing and cleaning of the conductive surface (e.g., steel), (ii) electroplating (with sacrificial or non-sacrificial anode), and (iii) post-treatment (rinsing and drying, phosphating, chromating, or oiling the surface)[68].

Although the primary result for the replacement of electroplated zinc by zinc foil showed promising results, further analysis needs to be done in this area to get the optimum result. The result from the battery made with the electroplated zinc shows that the battery does not deliver the same current capacity as the regular batteries. This might be due to the shortage of zinc particles in the battery. Since a zinc layer is coated on different substrates, drawing current from the battery will use up the zinc particles, and there will not be enough zinc on the substrate to run the battery. Cycle life with electroplated Zn anodes appears to pose additional problems. So far, we could not exceed 10 charge/discharge cycles.

Chapter 4

EXPERIMENTAL TECHNIQUES

In this section I will present the working principle of the main electrochemical techniques utilized in the framework of this Thesis. First, I will provide the basics of the instrumentation, and next will describe the methods. There are multiple techniques for measuring the performance of a battery. This section focuses on the measurement techniques used to characterize the charge capacity, cycle life, and internal of the galvanic cells fabricated throughout this Thesis work.

4.1 ELECTROCHEMICAL Instrumentation

Electrochemical instrumentation generally consists of a potentiostat, which imposes a controlled potential or current at one of the electrodes, termed the working electrode (abbreviated as WE). The potentiostat supplies power to enforce charge to the electrode, so that it can recharge secondary batteries.

Electrochemical workstations or potentiostats are instruments, which apply a known potential and monitor the current response to the potentiostat. In present, the most widely used potentiostats are assembled from discrete integrated-circuit operational amplifiers and other digital modules. In some larger instruments the potentiostat package also includes electrometer circuits, A/D and D/A converters, and dedicated microprocessors with memory. In other words, the potentiostat is a device that controls the potential applied across the working electrode-reference electrode pair, and it adjusts this voltage to maintain the potential difference between the working and reference electrodes [73].

The schematic of a potentiostat is shown in Figure 4.1. The system maintains the

potential of the working electrode (WE) at a constant level with respect to the reference electrode (Ref), by adjusting the current at a counter electrode (CE).

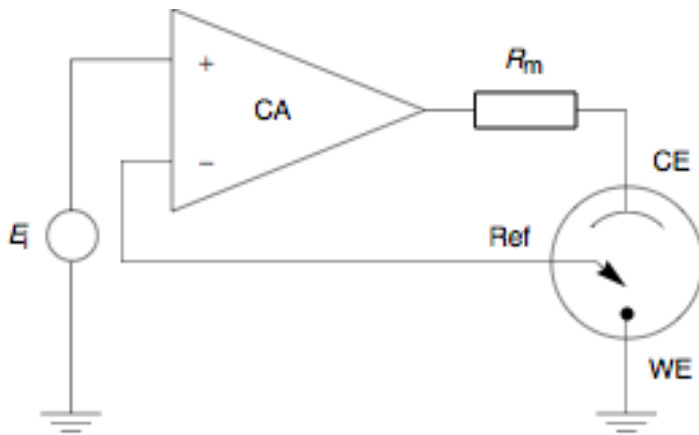


Fig. 4.1: Schematic of the potentiostat: the equivalent circuit of a 3-electrode cell (E_i is the input voltage, R_m - current-measuring resistor, and CA - control amplifier).

The potentiostat used through out this Thesis for battery testing is a Model VMP3 Electrochemical workstation, manufactured by BioLogic Scientific Instruments (Claix, France), it is a 16-channel multiplex instrument. The equipment uses a program function generator to run various experiments. The manufacturer’s software for this device is called EC-Lab, and it performs a variety of Electrochemical techniques from basic electrochemistry to corrosion/impedance measurements and battery test. Each of the techniques provides flexible user input, technique specific plotting formats, and data analysis tools [74].

EC-Lab offers more than 45 techniques that enable the user to address all Electrochemical applications. This software uses advanced graphic utilities. It provides two-axes representation on Y1 and Y2. It also allows the user to observe more than one graph in one window, and can monitor several parameters at same time. The simultaneous display of several graphs allows the user to follow an active experiment, while analyzing data acquired previously.

The software saves the setting for each channel and saves the data (in a so-called .mpr file format, which is the raw data file). These files can only be used by the BioLogic potentiostat software. We can also save data as a text file (in .mpt format), which can be imported into any text editor software.

4.1.1 Electrochemical Techniques Performed in 3-Electrode Geometry

Three electrodes are being utilized in these Electrochemical measurements, with the following role: the electrode of interest, referred to as the working electrode (WE), has a controlled potential set and monitored relative to the reference electrode (RE), while the current is passed between the WE and the counter or auxiliary electrode (both terms are being used in the scientific literature, and are abbreviated as CTR and AUX, respectively). The CTR (or AUX) electrode waives the RE from passing/handling large magnitudes of currents, which would be damaging to the RE.

In 3-electrode geometry the electrodes can be connected to the BioLogic potentiostat, as shown below:

- the electrode under investigation should be designated as the working electrode, and attached to the potentiostat by means of the red alligator clip;
- the counter electrode, typically a Pt wire electrode, is attached by means of the blue alligator clip, while
- the Ag/AgCl, 3mol/LKCl reference electrode, commonly abbreviated as Ag(RE), is clamped by means of the white alligator clip

4.1.2 Electrochemical Techniques Performed in 2-Electrode Geometry

For selected type of measurements, such as recording open circuit potential vs. time (ocP vs. time) or performing bulk electrolysis without potential control of the WE, this simpler 2-electrode geometry can be utilized. Most battery testing experiments are conducted in the 2-electrode geometry.

In this geometry, the WE will be utilized relative to CTR (or RE), where the counter electrode is connected to the RE. For zinc-RuO₂ cells the counter electrode is connected to the zinc, while the working electrode is attached to the graphite film, which serves as the current collector for the ruthenium side.

4.2 Electrochemical Techniques and Testing Procedures

This section summarizes different methods and techniques for battery testing. It also delves into different experiments used to determine various characteristics of a zinc-RuO₂ battery.

4.2.1 Cyclic Voltammetry (CV)

Beyond doubt, this is the most versatile, the most popular, and the best known Electrochemical method, with a wide range of applications from testing battery components to evaluating biological electron transfer, from determining corrosion rates to examining electrocatalytic properties of electrode materials. Also, CV is feasible for exploring various electroactive materials, from the gram-scale to the nano-scale. Given the wealth of its applications and the easiness of performing the analysis, one can consider cyclic voltammetry as the queen of electrochemical techniques.

The working principle of CV is presented in Figure 4.2, where the potential change vs. time, referred to as the *scan rate*, is imposed by the researcher, and the switching potentials are chosen according to the features of the system under investigation.

One important setting in CV is the so-called *sign convention*. The European sign convention displays the anodic peaks up and the increasingly oxidizing potentials from the left to the right, while the American or polarographic sign convention is exactly the opposite. For our workstation the setting of the instrument is according to the European sign convention, as shown in Figure 4.3.

4.2.2 Open Circuit Voltage

The open circuit voltage (ocV) measurements refer to a time span during which no potential or current is applied to the working electrode. In ocP mode the cell is not connected to any power amplifier. The evolution of the rest potential for the cell can be observed over time. This data can be used as preconditioning time or for equilibration of the Electrochemical cell [75]. Utilizing the zinc-RuO₂ cell with electrolyte of pH2.5 and a glass-fiber separator as an example, the nominal cell voltage is 1.4V. Therefore, the operating voltage of the cell will be from 1.4V to 0.6V, and the end voltage is typically 0.5V, for moderate and low-

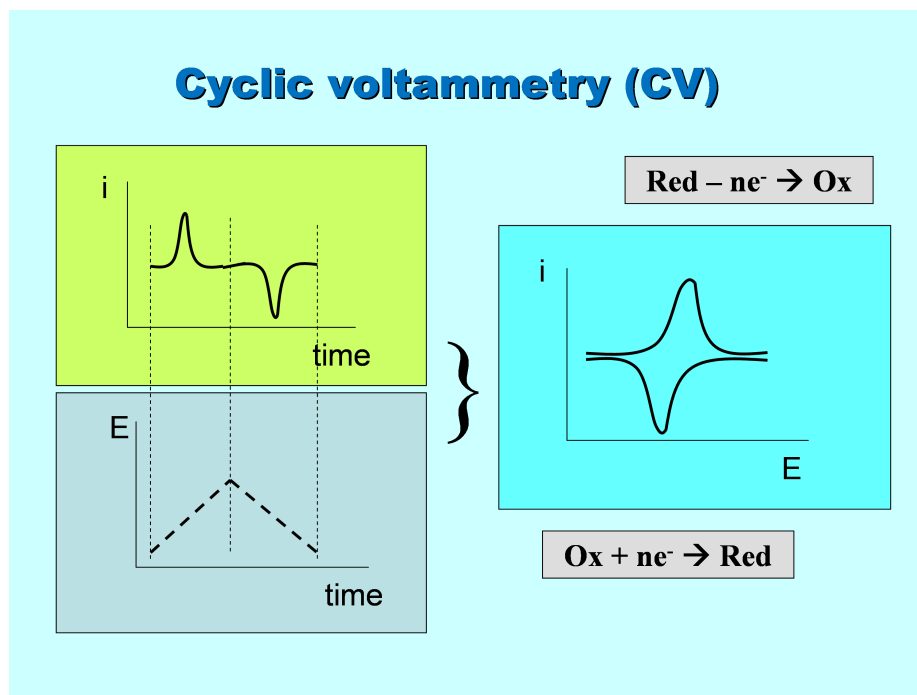


Fig. 4.2: Principle of cyclic voltammetry. In the left bottom panel the applied potential is displayed vs. time, and the current response vs. time is shown above it, while the right panel shows the output, the voltammogram in which current is plotted relative to the applied potential.

drain discharges, and $0.3V$, for engine cranking. The open circuit voltage of the $\text{Zn} - \text{RuO}_2$ battery is derived from the potential of the active anode and cathode materials, i.e., zinc and ruthenium (IV) oxide. The open circuit voltage depends also on the type of the ruthenium oxide (hydrated or anhydrous), and on the composition and pH of the electrolyte. As a result, the open circuit potential for a $\text{Zn} - \text{RuO}_2$ battery can be as low as $1.1V$ to as high as $1.5V$.

4.2.3 Charge /Discharge Studies

Different methods have been used to charge the battery, namely, constant current regime and constant voltage regimes. In these applications, charge and discharge sequences with possible open circuit periods can be measured. We can also look at the constant load discharge of a cell with different external loads. This is the most common test on a cell to determine its capacity. Furthermore, the life cycle of a cell can be explored. One can examine how the amount of charge going through a number of charge/discharge cycles can

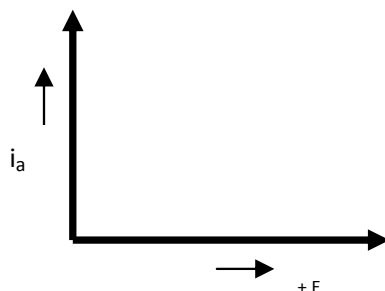


Fig. 4.3: European sign convention.

influence the performance of the cell. The battery will also exhibit self discharge over time that can be measured for a long time period.

Constant Current Charging

The title technique uses a constant current to charge the device under test, while monitoring the voltage across the cell. In order to charge the battery, a proper value for the current should be chosen. The battery undergoes the charging process, the voltage of the cell being monitored until it reaches a certain value. The voltage it stops changing over time. If the current is too low, then the overall charging process is very slow [76]. The described methodology is customarily applied for charging Li-ion batteries. If the current is too high, then it will generate excessive gas in selected types of batteries, due to the fast rate electrolysis of the supporting electrolyte inside the cell. One possible way of charging a battery using constant current regime is to apply to the battery a high current for a short time, and then charge the battery at lower current values over a longer time. This technique is called *two-step constant current charging*, which uses medium-to-high rate charge in the first period, followed by a very low current call trickle current, until the battery reaches full charge [76]. The advantage of using very small currents for charging a cell is evident, when a series of batteries are connected for charging. This allows the batteries to be rebalanced at the top-of-charge, i.e., at the nominal voltage of a cell, without causing any damage to the batteries that are already fully charged [76]. Overall, the constant current charging is a very slow process that can be considered for overnight charging.

Two sets of currents were used to charge the novel Zn – RuO₂ battery. Figure 4.4 shows

the charging curve for the current set to $240\mu A$. The charging process takes $3h$ and $30min$, until the battery reaches the nominal voltage of $1.15V$, and the voltage flats out at that voltage.

By comparison to the previous set up, a second test uses $50\mu A$ constant current to charge a battery, which leads to a longer charging time. In this process, it takes for $8h$ and $30min$ to charge a battery to the constant value of its nominal voltage. Figure 4.5 displays the charging curve for this method.

Since the batteries had been discharged several times the initial nominal voltage of $1.4V$, could not be reached. The maximum current provided by the potentiostat was only $240\mu A$, therefore, excessive time was needed to charge up the battery, and, also, the highest potential could not be reached.

Comparing the two techniques, one can see that when the higher current is used to charge a battery, the faster the charging voltage will achieve its highest point. The smaller current can also be useful when time is not the main concern.

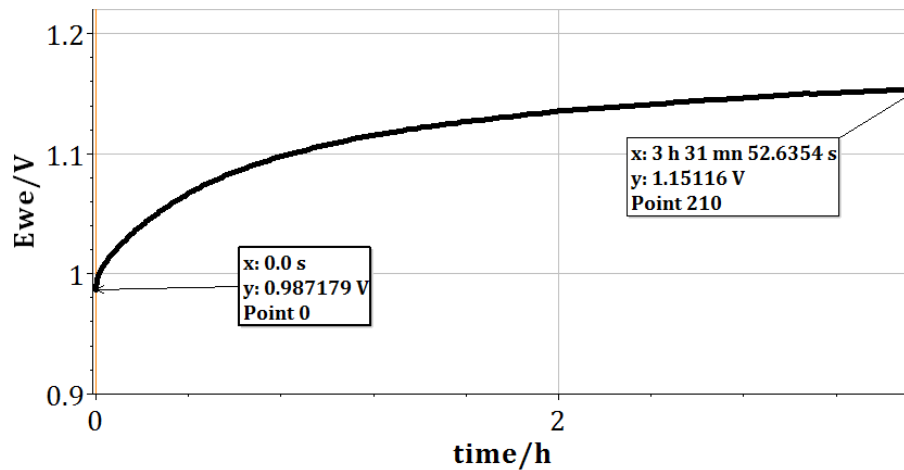


Fig. 4.4: Constant current charging with $240\mu A$ current.

Constant Voltage Charging

As the name implies, this regime involves the use of a constant voltage throughout the charging process. The current starts off at a very high value, and then decreases almost exponentially to a low value. When the battery is deeply discharged, the starting current

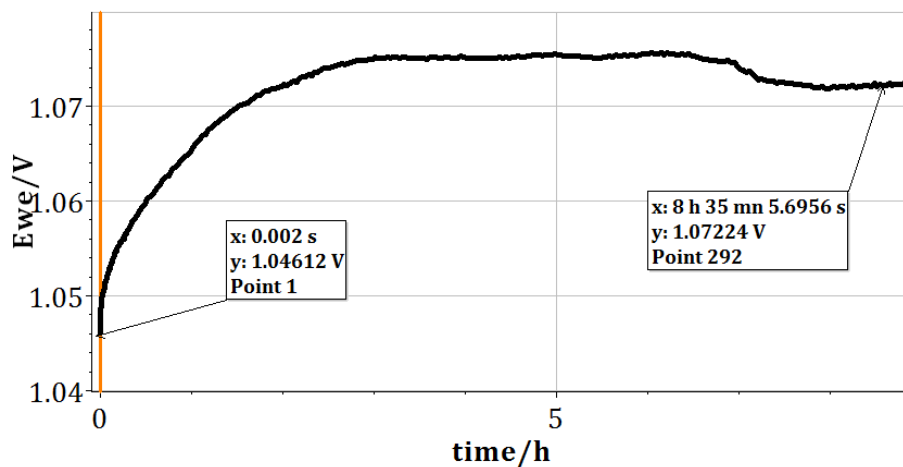


Fig. 4.5: Constant current charging with $50\mu A$ current.

can be very high; this may result in internal heating of the cell. Figure 4.6 is an example of current-time curve, when the Zn – RuO₂ battery is charged with 1.4V for 1h. As the plot implies, the charging current starts as high as 74mA, and drops to 0.062mA in 1h. Depending on how deep the battery was discharged previously to the charge, the initial current and the time needed for the current to drop to very low values may vary. Further studies are needed on the charge time of a battery for reaching an accurately set potential value.

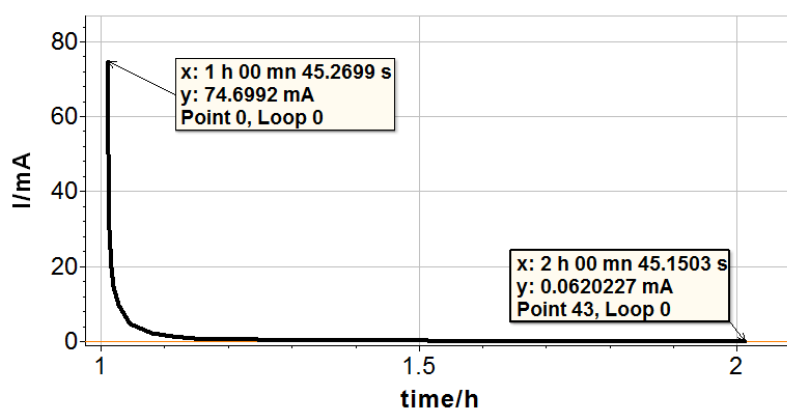


Fig. 4.6: Constant voltage charge current of a Zn – RuO₂ cell, when charged at 1.4V for 1h

Constant voltage charging can be used as a fast technique for returning maximum charge in a minimum time [76]. The starting potential, when a battery is charged at a certain potential, will be the same as the charging voltage under normal conditions. For example,

if a battery is charged at $1.4V$, then the starting voltage after the charging will be $1.4V$, as well.

Constant Load Discharge

Constant load discharge (CLD) is the technique to measure the total capacity of a cell. As explained in section 4.1, the BioLogic potentiostat allows the user to set the load. Constant load discharge implies that the load resistance stays constant throughout the discharge for specific duration of time. The magnitude of the external load used for testing the battery mainly depends on the application of the battery. If the battery needs to provide a large burst current in subsequent a short given time, then smaller load resistance is used. By contrast, when it is needed to source small constant current over a longer time period, then a greater load resistance will be used to test the performance of the battery. The charge capacity of a galvanic cell can be expressed in Ah or mAh units. To calculate the capacity of a cell constant load discharge technique is used. Figure 4.7 shows an example of constant load discharge of a cell for measuring its capacity.

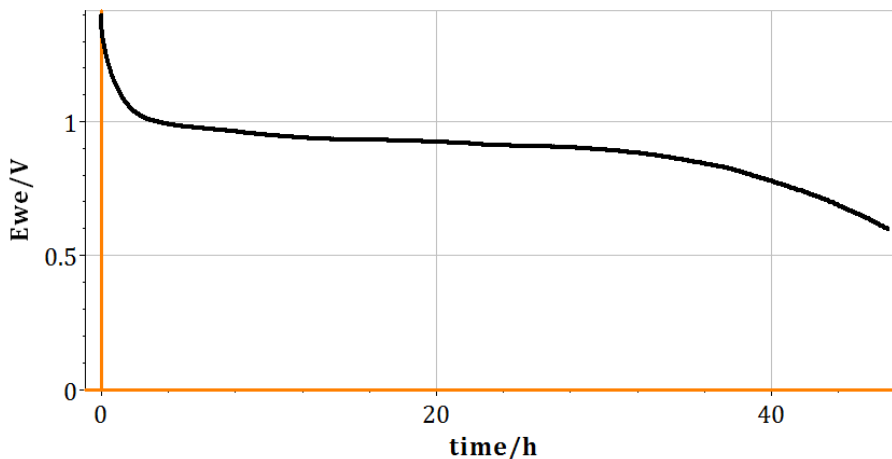


Fig. 4.7: Constant load discharge of a battery through $1k\Omega$ external load, providing a charge capacity of over $10mAh/cm^2$.

Constant Current Discharge or Chronopotentiometry

Chronopotentiometry (CP) is a controlled current technique. The current is controlled, and the potential is the variable determined as a function of time. This technique is mostly used

when one is interested in the performance of a cell as a response to a pulse. CP technique enables for the monitoring of the potential of a cell, when specific amount of current is drawn over time. Figure 4.8 shows an example of using this technique, when the potentiostat is set up to draw specific current for a particular time period, while monitoring the voltage. The magnitude of 0.1mA current was drawn from a cell for 30s , and the potential of the cell was monitored. As will be explained in subsection 4.2.5, the CP can be used for internal resistance testing or for the experiments or for protocols where an exact magnitude of peak current is required.

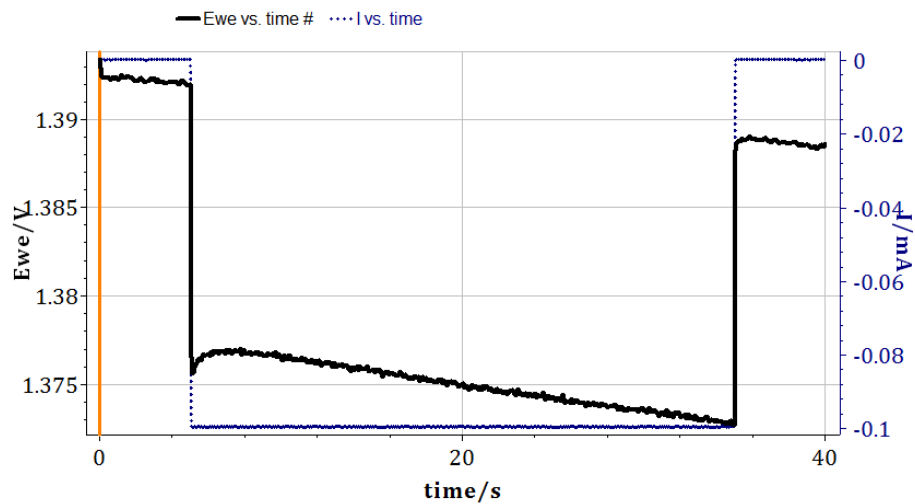


Fig. 4.8: Voltage vs. time discharge recorded by CP for calculating the internal resistance of a cell.

Cycling

Rechargeable batteries, also known as secondary cells, are batteries with reversible electrochemical reactions, which allow for reversible electrical operation of the cell. Ruthenium (IV) oxide is an example of a cathode that can be used in rechargeable batteries. The number of cycles that a battery is able to perform is referred to either as cycleability or cycle life. To test this feature, the battery should be discharge through a constant load for a certain duration, and then recharged. The charge time depends on both the load and the depth of the discharge. In this Thesis, the typical cycleability test is 1h discharge of a cell through $1\text{k}\Omega$ load, followed by 1h charging at 1.4V potential. Figure 4.9 is an example

of approximately 100 full 1h cycles achieved with a 4cm^2 Zn – RuO₂ cell. As the plot reveals, the voltage slowly decays as the number of cycles increases. What is desired from a secondary battery is to be able to undergo a number of discharges, while maintaining the dropping potential constant.

Figure 4.10 shows the amount of charge that was drawn from the battery in each cycle. On the average, the battery is able to source 0.9mA.h. Further investigation shows that 95 cycles have the current capacity above 80% of the capacity of the first four cycles.

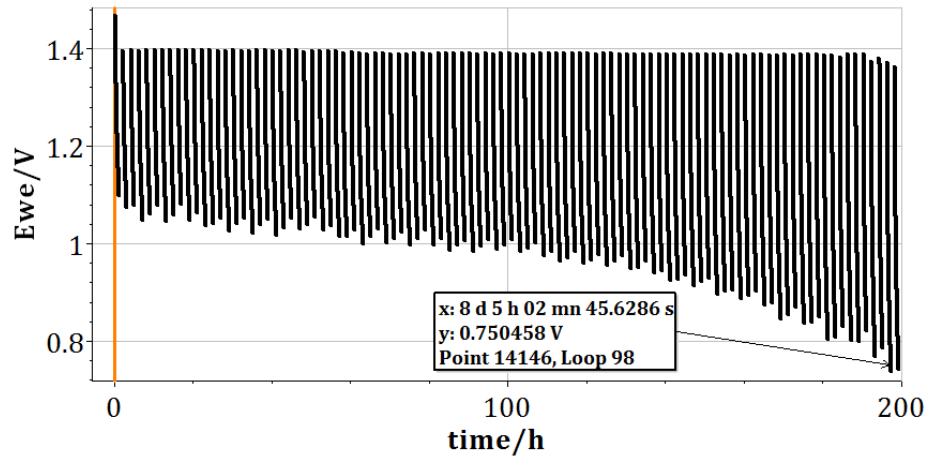


Fig. 4.9: 100 cycles accomplished from a 4cm^2 Zinc-RuO₂ battery with $1k$ load and $1.4V$ charging intervals.

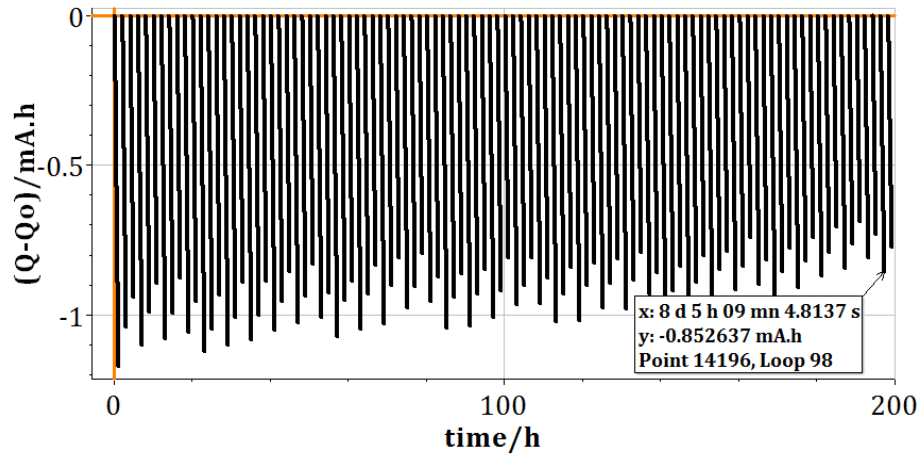


Fig. 4.10: The capacity plot drawn from a 4cm^2 Zn-RuO₂ battery

The battery is not able to accomplish cyclability exceeding 100 cycles for discharges 1h duration through $1k\Omega$ load. More cycles can be accomplished with smaller rate load and

faster discharges. Figure 4.11 shows the completion of 800 cycles that involve very short discharge intervals of 1min discharges with 3min charges.

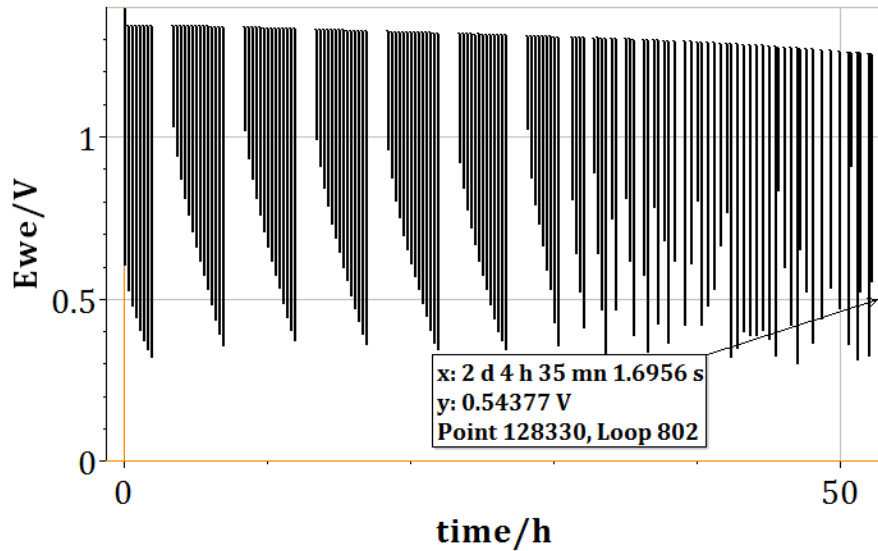


Fig. 4.11: 800 cycles accomplished by the Zn – RuO₂ battery.

Listed below are some considerations with regards to cyclability for zinc batteries. It is difficult to accomplish a large number of cycles with zinc anodes [77]. There are three main reasons for this inability:

1. The material tends to form dendrites that pierce the separator, and short out the galvanic cell;
2. There is a “*size effect*,” whereby the zinc surface changes shape during discharge–charge cycles. Zinc clumps in one area, and disappears from others. This leads to current crowding, local heating, and the eventual destruction of the electrode; and
3. Formation of insoluble zinc oxides.

Further studies have been done on the above features for solving these problems. The zinc particles need to be kept in place, and chemical reactions should proceed on the zinc surface. The goal is to protect zinc from surface corrosion. Different additives have been tested to keep the zinc particles in place, which is beyond the scope of this Thesis.

4.2.4 Shelf Life/Self-Discharge

Shelf life of a cell is defined as the length of time over which the battery maintains its potential and capacity, when not in use. The shelf life of a cell is directly tied to the extent of its self discharge. In other words, the time period that battery is being stored and still is suitable for operation there after that depends on how much the battery is going to discharge without being connected to a load, i.e. in open circuit mode. Our experimental findings show that self-discharge of a cell in the Zn – RuO₂ battery depends primarily on electrolyte pH. Near neutral pH, the cell shows very low self-discharge. Figure 4.12 reveals the low self-discharge for a $4 \times 4\text{cm}^2$ battery discharged through $50\text{k}\Omega$ load, over three months. A negligible drop in cell voltage occurred.

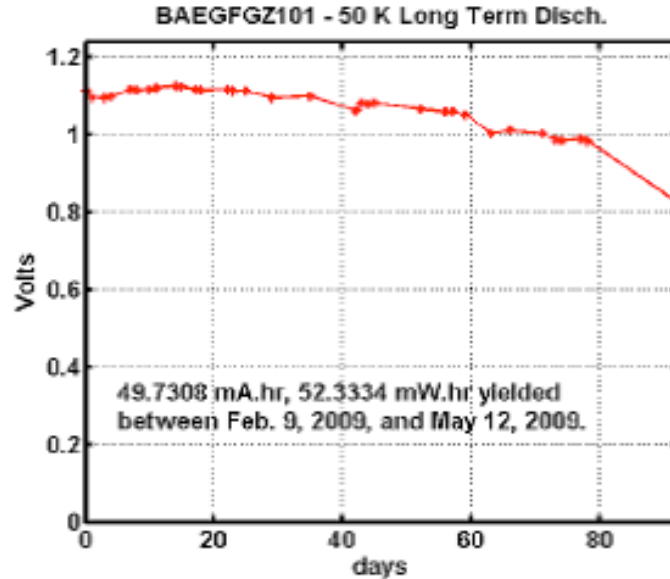


Fig. 4.12: Three-month discharge of a cell with 16cm^2 of active area, operating with electrolyte of near neutral pH.

As shown in subsection 5.1.2 the acidic pH enables for higher current capacity, owing to the lower internal resistance of the cell. There is a trade-off that we should keep in mind, while choosing the electrolyte, although the lower pH has smaller internal resistance, it increases self-discharge of the cell. In other words, whenever an electrolyte is Electrochemically active, it typically is active in the purely chemical process, as well, i.e., it speeds up the corrosion of the zinc electrode, and by this it decreases shelf life. We will need to

optimize the cell system with this trade-off in mind.

A series of batteries have been tested for shelf life and self-discharge. These batteries were made with electrolyte having the pH of 2.50 ± 0.05 and the active area of $2\text{cm} \times 2\text{cm}$. Four such batteries were connected in series as part of a battery cloth. The potential of the battery was monitored over time, and plotted as shown in Figure 4.13. A comparison between the performance of these two batteries reveals that the cell with the close to neutral pH has a 27% drop in potential over 90 days, while the battery with the more acidic pH has dropped by 38% in 64 days. For the same time period of 64 days the battery with the neutral pH has dropped only by 9%.

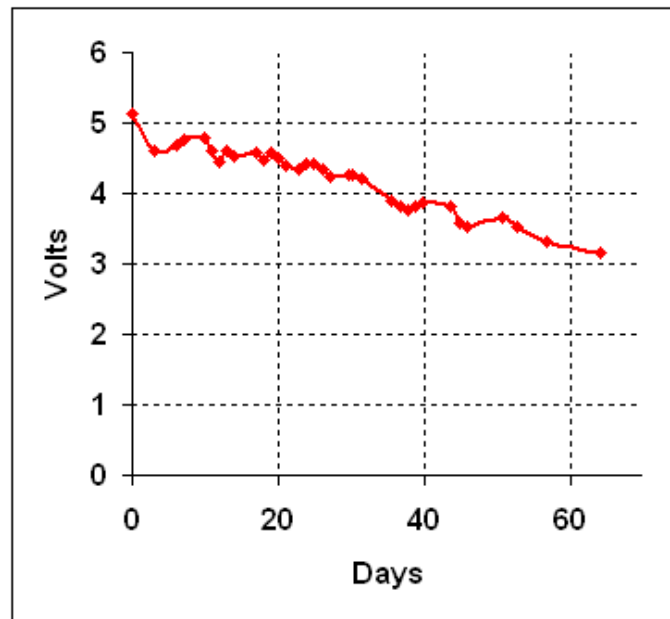


Fig. 4.13: Two months discharge of a 5V cell with 4cm^2 of active area and acidic pH.

4.2.5 Internal Resistance

The internal resistance of a battery, also called equivalent series resistance (ESR), is defined as the “force” opposing to the flow of current within the battery [78]. Any electronic device that generates voltage can be represented by an ideal voltage source with impedance in series with it. Considering the time dependency of the cell behavior, the ideal voltage source can be in parallel with a capacitor. The impedance is called the internal resistance of a battery. Figure 4.14 illustrates the model for a battery.

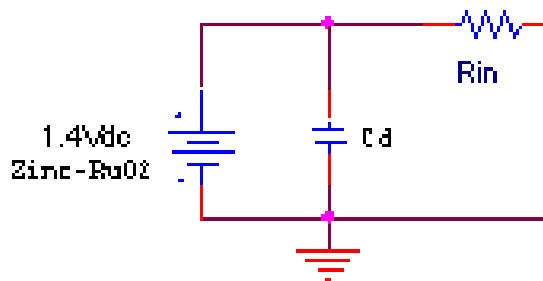


Fig. 4.14: The equivalent circuit of a battery.

There are two factors that impact the internal resistance of a cell. They are the electronic resistance and the ionic resistance [78]. The summation of these two resistances is called the total effective resistance of a battery. The ionic resistances are due to various Electrochemical parameters, such as electrolyte conductivity, ion mobility, and the surface area of electrodes [78]. These factors affect the performance of the cell to a lesser extent than the electronic resistance. These factors typically act when the battery is connected to a load. Electronic resistance also influences the performance of a battery. Rather than being internal, the electronic resistance is mostly due to the connection of a battery to other devices.

Figure 4.15 shows the experiment done on the novel ruthenium oxide cell to calculate its internal resistance. For 5s a battery was in open circuit, hence, no current was drawn from the battery. In the meanwhile, the voltage over time was monitored. Then, over the next 30s larger magnitude of current was drawn from the cell. In this step, the battery was set up to source $100\mu A$ current. Using Ohm's law the internal resistance of the battery can be calculated by dividing the drop in voltage by the change in current. This yields the internal resistance of 5Ω .

In order to get more accurate results on the internal resistance of the cell, this experiment needs to be repeated for different current ranges. chapter 5 looks into the internal resistance of the batteries, when different parameters of the battery (such as electrolyte of separators) were changed.

As explained above, different parameters will influence the internal resistance. Therefore, the material used in the cell, e.g., filter paper separators, will largely affect the internal

resistance. Same technique has been used to calculate the internal resistance of a cell in chapter 5.

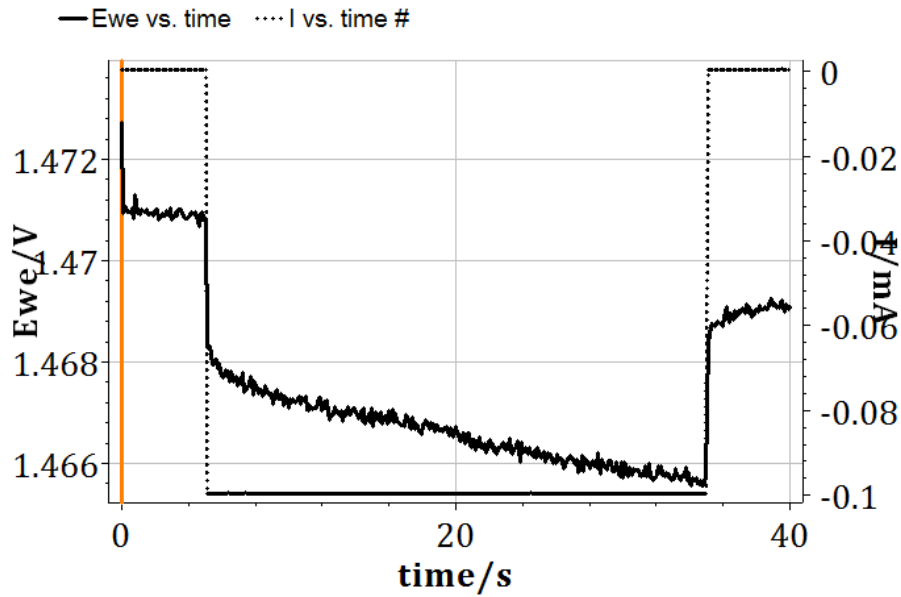


Fig. 4.15: Calculating the internal resistance of a cell by using CP technique; it yields the value of 5Ω .

As described in chapter 3, a simpler form of the cathode reaction is as shown in equation (4.1):



It is possible for a cell with an acidic electrolyte to exhibit the reaction according to equation (4.2):



The formation of hydrogen gas also adds to the internal resistance of a cell. Creating a hydrogen bubble enforces ions to avoid the bubbles, by traveling around the gas bubbles, as opposed to going in straight directions. This phenomenon will lower the rate of ion migration, and result in the increase of the internal resistance.

Chapter 5

MEASUREMENTS AND TESTING RESULTS

As described throughout this Thesis different parameters will affect the performance of a battery. This section looks into the performance of a Zn – RuO₂ battery when different parameters are being changed in the battery. The battery performance has been analyzed when different pH electrolytes as well as different separators and anode materials are used.

5.1 Electrolyte Effects Measurements

The effect of electrolyte on the battery performance has been described previously. This section demonstrates the batteries' capacity when electrolytes of different pH values are used. Different materials are used to make an electrolyte. Some of the electrolytes consist of same materials with different amounts of acid added to adjust the pH. The battery with highest current capacity of 33.35mAh/cm^2 was made with the mixture of zinc chloride (ZnCl₂) and ammonium chloride (NH₄Cl) and uses hydrochloric acid (HCl) to adjust the pH. Basic electrolytes with higher pH were made with the zinc acetate family, which did not provide outstanding results.

5.1.1 Original Electrolyte

The original cell was implemented with an electrolyte composed of a weak acid and ethylene glycol that is close to neutral pH, to prevent rapid dissolution of the electrode materials or package sealing materials, while providing the needed redox reactions. For the original standard electrolyte a mixture of boric acid, citric acid and ammonium hydroxide mixed with ethylene glycol was used. The charge capacity accomplished with this electrolyte was

0.0325mAh/cm². As part of the improvements for the performance of the battery, different types of electrolytes with different compositions and different pH were used.

5.1.2 Overview of Electrolytes of Different pH Value

As shown above, the composition and pH of the electrolyte will affect battery performance significantly. Listed in Table 5.1 are the compositions and pH values of various electrolytes tested in Zn – RuO_x batteries. The second column displays the internal denomination of each electrolyte, while column 4 shows the best charge capacity accomplished with each electrolyte.

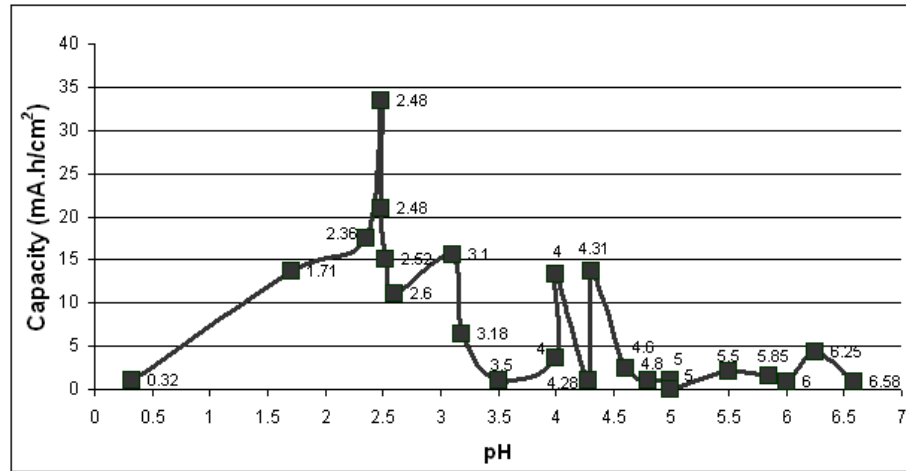


Fig. 5.1: Plot of battery capacity versus pH for different electrolytes. Note that connecting point is just for visual clarity.

As the plot in Figure 5.1 illustrates, at pH 2.48 of the electrolyte, the galvanic cell reached the maximum capacity of 33.35mAh/cm². This electrolyte (E10A4) was made with a mixture of zinc chloride and ammonium chloride, both salts used at high concentrations, the pH of the solution being adjusted with hydrochloric acid. Another battery was made with a different salt mixture, at the same pH of 2.48. The latter electrolyte (E10A5) contained a ternary salt mixture: zinc chloride, ammonium chloride, and zinc acetate. Batteries made with the latter electrolyte delivered high current capacity, but not as high as with the E10A4 electrolyte. Other high capacity points were recorded at pH ranges from pH 1.7 to 3.1. Also, at the pH of 4 and 4.3, the capacity values were slightly less than half of the maximum accomplished point.

Salt Composition	Electrolyte	pH	Capacity (<i>mAh/cm²</i>)
Boric Acid, Citric Acid, NaCl	E05	0.32	1.11
ZnCl ₂ , NH ₄ Cl	E10A2	1.71	13.75
ZnCl ₂ , NH ₄ Cl	E12	2.36	17.5
ZnCl ₂ , NH ₄ Cl	E10A4	2.48	33.35
ZnCl ₂ , Zn(C ₂ H ₃ O ₂), NH ₄ Cl	E10A5	2.48	21
ZnCl ₂ , Zn(C ₂ H ₃ O ₂), NH ₄ Cl	E12A	2.52	15
Zn(C ₂ H ₃ O ₂) ₂ , NH ₄ C ₂ H ₃ O ₂	E16B	2.6	11.04
ZnCl ₂ , NH ₄ Cl	E12B	3.1	15.67
ZnCl ₂ , NH ₄ Cl	E10A1	3.18	6.43
ZnCl ₂ , NH ₄ Cl	E10A	3.5	1.03
Zn(C ₂ H ₃ O ₂) ₂ , NH ₄ Cl	E014A	4	3.67
ZnCl ₂ , NH ₄ Cl	E12C	4	13.37
Zn(C ₂ H ₃ O ₂) ₂	E013A	4.28	1.11
ZnCl ₂ , NH ₄ Cl	E10A3	4.31	13.7
Zn(C ₂ H ₃ O ₂) ₂ , (NH ₄) ₂ SO ₄	E015A	4.6	2.41
Zn(C ₂ H ₃ O ₂) ₂ , NH ₄ C ₂ H ₃ O ₂	E16A	4.8	1.04
ZnCl ₂ , NH ₄ Cl	E10B	5	1.12
Boric Acid, Citric Acid	E01	5	0.032
ZnCl ₂ , NH ₄ Cl	E11	5.5	2.12
Zn(C ₂ H ₃ O ₂) ₂ , NH ₄ Cl	E014	5.85	1.48
Zn(C ₂ H ₃ O ₂) ₂	E013	6	0.78
Zn(C ₂ H ₃ O ₂) ₂ , (NH ₄) ₂ SO ₄	E015	6.25	4.27
Zn(C ₂ H ₃ O ₂) ₂ , NH ₄ C ₂ H ₃ O ₂	E16	6.58	0.8

Tab. 5.1: Denomination of different electrolytes with different pH value and the charge capacities enabled by them. All batteries were made under similar conditions and testing environment.

As column one of the table implies, the electrolytes were made with different salt compositions, at different molarities of the salts, which are not mentioned in this Thesis due to the confidentiality of the material. Figure 5.2 provides a relevant correlation of charge capacity and pH, as it shows electrolytes that belong to the same family of salts. The electrolytes were made with different molarities of zinc chloride and ammonium chloride.

As shown in the plot, the electrolytes made with zinc chloride and ammonium chloride have high current capacity except for pH greater than 5.

In an attempt of explaining the outstanding performance of the electrolytes, which contain zinc salts, we hypothesize an equilibrium process between the metallic zinc, which is the anode material, and the hydrated zinc ions, present in the electrolyte, according to equation (5.1):

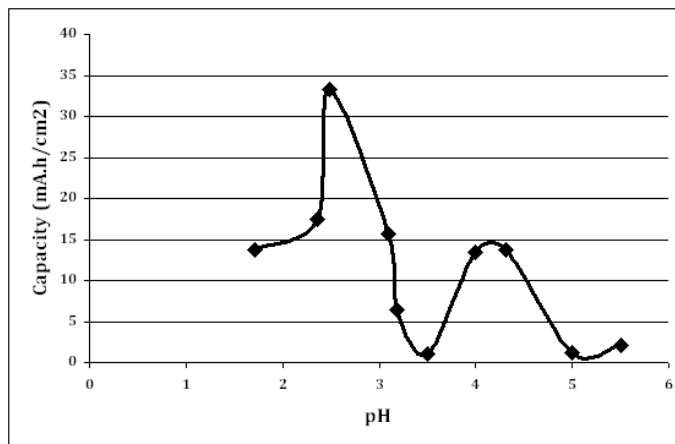
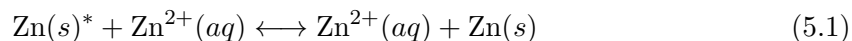


Fig. 5.2: Capacity versus different pH values of the electrolytes that belong to the same family; they all contain different concentrations of zinc chloride and ammonium chloride. Note that connecting point is just for visual clarity.



Where * marks the metallic zinc, which constitutes the anode. This equilibrium may control the dissolution of metallic zinc from the anode, and the zinc ions added to the electrolyte is likely to limit the extent and rate of metallic zinc dissolution. Therefore, the equilibrium shown in equation (5.1) improves the charge capacity and the cycle life, while it also extends the shelf life of the galvanic cell.

In addition, the high concentration of salts present in the zinc salt based electrolytes confers good ionic conductivity to the system, which limits the magnitude of unwanted ohmic drops in the cell. Our most recent experiments revealed that not the highest concentrations of zinc and ammonium salts are the most efficient. Upon reducing the Zn^{2+} salt concentration to by 1/3 and the NH_4^+ to approximately 1/2 of that used in E010A4, the charge capacity of the battery has increased. We believe that this finding may be a consequence of a good compromise between the conductivity of the electrolyte and its lesser salt concentration, which prevents the dry out of the cell.

5.2 Cathode Current Collector

We represent here the performance of the Zn – RuO_x battery, when different current collectors are utilized. Table 5.2 shows the thicknesses of different current collectors, their Ohmic resistance, and their performance in battery operation.

Cathode Current Collector	Thickness (<i>mm</i>)	Internal Resistance (Ohm)	Capacity (<i>mAh/cm²</i>)
Carbon Mesh	0.26	82	58
Carbon Veil	0.10	57	30
Carbon Cloth	0.30	66	35
Buckeye	0.10	140	50
Graphite sheet	0.13	40	34

Tab. 5.2: Different current collectors.

It can be observed that the carbon mesh is delivering the highest capacity of 58mAh/cm^2 . However, it also has the greatest thickness among the current collectors, and this prevents accomplishing our goal. The buckeye paper has higher capacity than the graphite sheet. However, purchasing these materials is currently not cost efficient. Buckeye paper is 7 times more expensive than that of graphite.

Graphite sheet possesses two advantages over other materials. First, it is easier to work with it and is uncomplicated to handle, as compared to carbon veil or buckeye paper. Those materials are fragile and often break. Therefore, on the lab scale, where batteries are hand-made, the handling of graphite sheet is easier than of other materials. Second, graphite sheets exhibit the lowest internal resistance of 34 Ohm.

Table 5.3 illustrates the nominal continuous current for each of the tested current collectors. As the table reveals, although graphite mesh has the highest capacity, its nominal continuous current is 35% less than that obtained with graphite sheet. It can also be observed that the battery with graphite sheet has high nominal current, same as the case with buckeye and carbon cloth, although the capacity is lower.

5.3 Separator Analysis

This section looks into the effect of separators on the performance of the batteries. The capacity of a cell has been analyzed, and its internal resistance and cyclability, as well.

Cathode Collector	Nominal Continuous Current (mA)
Carbon Mesh	0.74
Carbon Veil	0.54
Carbon Cloth	0.86
Buckeye	0.84
Graphite sheet	0.84

Tab. 5.3: Nominal continuous current for different cathode current collectors

Various separators with different thickness were used in making the batteries.

Table 5.4 lists some separators obtained from commercial suppliers, each having a different thickness and a characteristic performance. All batteries contained the same electrolyte, with the acidity pH set to 2.43, and were made under similar conditions. The thickness of a cell versus its capacity as well as its internal resistance and the number of cycles were measured.

Name	Thickness (μm)	Capacity (mAh/cm^2)	# of Cycles	Internal Resistance (Ω)
F&J Specialty	350	33.35	40	32
Fisher Scientific	240	20.30	61	73
Whatman	216	12.5	68	65
AMC	100	10.5	33	61
KIMTECH Wipes	60	7.87	20	29
Celgard	20	9.87	2	72

Tab. 5.4: Different separators with different thickness and their performance in capacity, number of cycles, and internal resistance.

Figure 5.3 shows the thickness of the utilized separator versus the capacity of the cell. As it can be seen, the thicker the separator, the more capacity can be drawn. This may be a consequence of more electrolyte absorbed by the thicker glass-fiber separator.

The batteries with different separators also underwent cycling test. The cycling tests for these batteries were recorded as described in chapter 4. Figure 5.4 is the plot of the separator thickness versus the number of cycles. The cycleability of a battery was based on the number of 1-hour cycles it underwent over a $1k\Omega$ external load. As the result implies, unlike the capacity test the separator thickness is not proportional to the number of cycles and the separator with $216\mu m$.

The internal resistances of cells related to different separators were also measured ac-

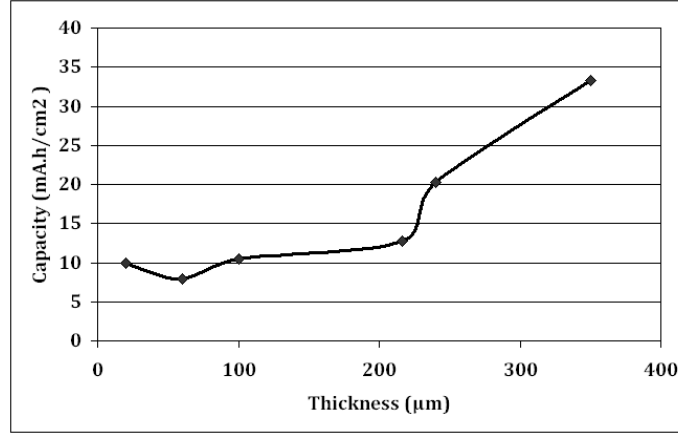


Fig. 5.3: Capacity versus the thickness of a separator obtained from Zinc-RuO₂ battery system. Note that connecting point is just for visual clarity.

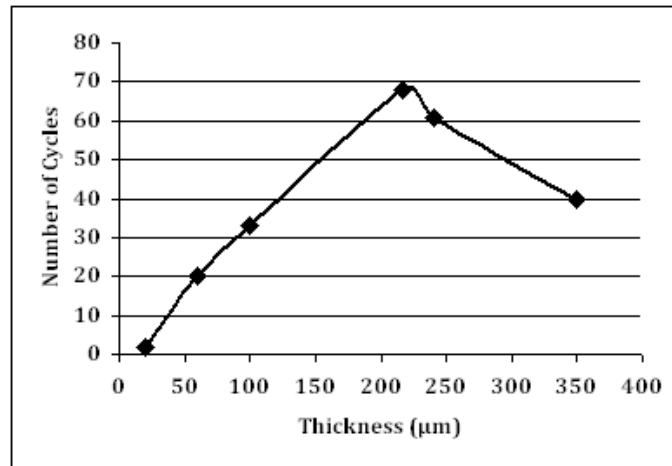


Fig. 5.4: Number of cycles versus the thickness of a separator obtained from the Zn – RuO₂ battery system. Note that connecting point is just for visual clarity.

According to the procedure discussed in subsection 4.2.5.

The internal resistance is not necessarily related to the separator thickness. As the plot in Figure 5.5 shows, the KIMTECH wipes have a very small internal resistance, while the capacity of the cell and its number of cycles are not the best.

One important factor that we need to keep in mind while comparing the separators is that not all separators tested by us belonged to the same family. The F&J and the Fisher Scientific separators are made of glass-fibers, while Celgard is based on polypropylene layers. The membrane material for AMC is modified hydrophilic polyethersulfone.

The above considerations are of important qualitative value. Their quantitative infor-

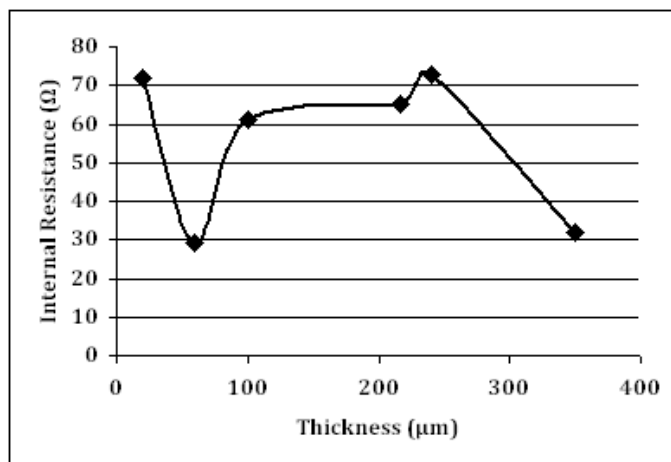


Fig. 5.5: Internal resistance of a cell versus the different separators thickness. Note that connecting point is just for visual clarity.

mation is hindered by the fact that we were not able to make the same type of battery at different thicknesses. The unavailability of different thicknesses of separators having the same composition prevented a more accurate comparison.

5.4 Anode Materials

While ruthenium is a novel material used as a cathode in this study, zinc and aluminum batteries have been known for decades. As described in subsection 3.1.2 the reaction on the anode side is quiet simple. However, the reduction potential of the anode will determine the cell voltage. In this section, I present my analysis of the performance of the Zinc-RuO_x and Al – RuO_x batteries.

5.4.1 Zinc-RuO_x Batteries

The capacity and cycle life for the zinc battery is demonstrated here. Typically, batteries were made with 0.6mm thick zinc as the anode and a mildly acidic electrolyte, having pH2.48. The electrolyte was the combination of a zinc salt and an ammonium salt, in most cases both were chlorides. The pHof the electrolyte was adjusted by adding rigorously controlled amounts of an acid (HCl, H₂SO₄, or acetic acid). The separator was glass-fiber from F&J Company; it had the thickness of 350μm. The battery provided 33mAh/cm² ,

when connected to a $1k\Omega$ external load.

A battery with the same characteristics was made for testing the cycling ability of the cell. The battery was discharged through $1k\Omega$ load for $1h$, and then charged at the applied voltage of $1.4V$ for another hour. The goal was to assess the number of cycles the battery is able to provide charge, i.e., how long it can cycle consistently. The battery went through 98 cycles before it hit the pre-set end potential of $0.7V$. Figure 5.7 shows the cycling of the battery. Currently, the desired cycle life for the secondary battery is not yet achieved. The battery dies after a number of cycles because of (i) the formation of gas bubbles that affect the battery membrane, and increase the internal ohmic resistance of the galvanic cell, and (ii) the dry out of the cell; a very small volume of electrolyte is added to the cell, which is eventually lost by electrolytic decomposition and evaporation.

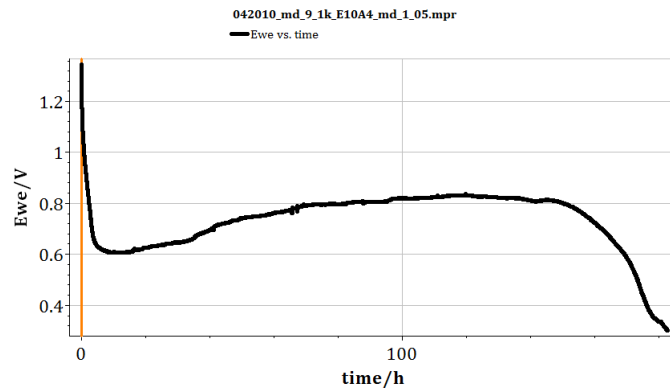


Fig. 5.6: Discharge curve for Zn – RuO₂ battery with pH2.48 electrolyte over $1k\Omega$ load

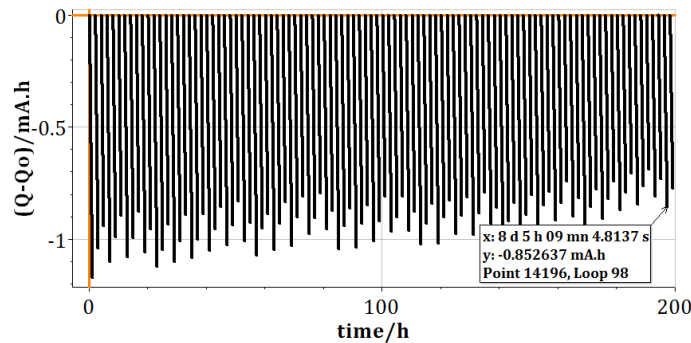


Fig. 5.7: Approximately 100 cycles accomplished with Zn – RuO₂ battery through $1k\Omega$ load with charging cycle in between two discharges, at an applied voltage of $1.4V$.

5.4.2 Al – RuO_x Battery

As explained in section 2.4.1, Al can be used as an anode in the RuO_x cells. We employed two different electrolytes to make the Al cells. One with pH6.2, containing boric acid, citric acid, and ethylene glycol. The battery was not able to deliver more than 102 μ Ah before it dropped to a very low voltage and died. Figure , shows the voltage curve of the battery. The battery has the initial potential of ca. 1V. Another strongly acidic electrolyte, with pH \sim 0.2 was used to test the Al – RuO₂ battery. The electrolyte has the same composition as previously, except that it also contains hydrochloric acid. Figure 5.8(b) shows the discharge curve for this battery. The battery had higher initial voltage than the battery with greater pH.

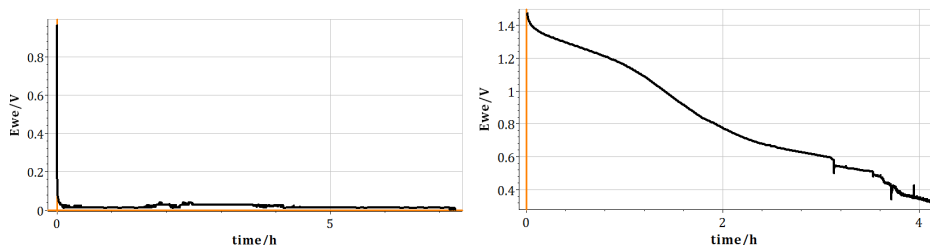


Fig. 5.8: (a). Discharge curve for the Al – RuO₂ battery with pH6.2 electrolyte. (b). Discharge curve for the Al – RuO₂ battery with pH0.2.

5.5 Monitoring Hydrogen Discharge and Water Decomposition by Cyclic Voltammetry in Open Cell Experiments

The goal of this investigation was to determine the potential window in which each electrolyte is stable, and to get a preliminary diagnostics on gas evolution, in both the cathode and anode reaction. The technique described here enables for examining in a systematic manner the effect of pH on gas formation.

We tested several electrolytes that we customarily utilize in the galvanic cells, as follow: E010A4 (pH-0.15), E010A5 (pH1.64), E010A7 (pH2.40), E013 (pH5.68), E014 (pH5.85), and E030A (pH2.26).

Tests were performed by cyclic voltammetry (CV), in 3-electrode geometry. The working electrode was graphite film. Metallic zinc plate was the counter electrode, and Ag/AgCl, 3MKCl, abbreviated as Ag(RE), served as the reference. This setup can be extended to the use of working electrodes identical to those employed in sealed galvanic cells, namely, hydrated Ru(IV) oxide confined to graphite support

Cyclic voltammetry was recorded in a 10mL glass cell, which contained 5mL of electrolyte, and the above electrodes were immersed into the liquid. Measurements were performed at room temperature, without degassing the electrolyte. CV scans were recorded in an increasingly wide voltage window, e.g., from the initial $-0.6V$ to $+0.8V$ to the more and more positive upper value concomitant with the more and more negative limit. The scan rate was kept at moderately fast value (at or around $100mV/s$). CV scans will be recorded at identical scan rate, at room temperature, and without degassing the electrolyte solutions. These conditions are comparable to the ones in the FlexEl galvanic cells. Therefore, the ex situ experiments are expected to be relevant to our real life batteries.

Scans recorded so far showed that the negative limit of the voltage range typically cannot be pushed below $-1.15V$, while the upper limit can be as high as $+1.3V$ or even more positive. It was also demonstrated that metallic zinc cannot serve as the working electrode (given that it behaved as an ideally non-polarizable electrode), but it can be used as the counter electrode. This setting corresponds to the setting of the two electrodes in the galvanic cell.

Figure 5.9 displays an overlay of two CV scans recorded for electrolyte E10A5, in a potential range, which has the same upper limit, but a slightly different negative potential limit. One can notice a striking difference, when the negative end of the scan is extended by only $100mV$; while at $-1.05V$ vs.Ag(RE) no hydrogen evolution occurs, at $-1.15V$ vs. Ag(RE), strong hydrogen discharge proceeds.

In E010A4 electrolyte ($pH < 0$), strong hydrogen evolution occurred, as soon as the zinc plate was immersed in the solution. It looked like boiling water. Hence, open cell experiments reveal the same behavior of zinc in electrolytes, as evidenced by the ex situ zinc corrosion experiments. Potential windows for various electrolytes are listed in Table 5.5. The pH value of the electrolyte was measured with a Model SevenEasy pHMeter (Toledo-

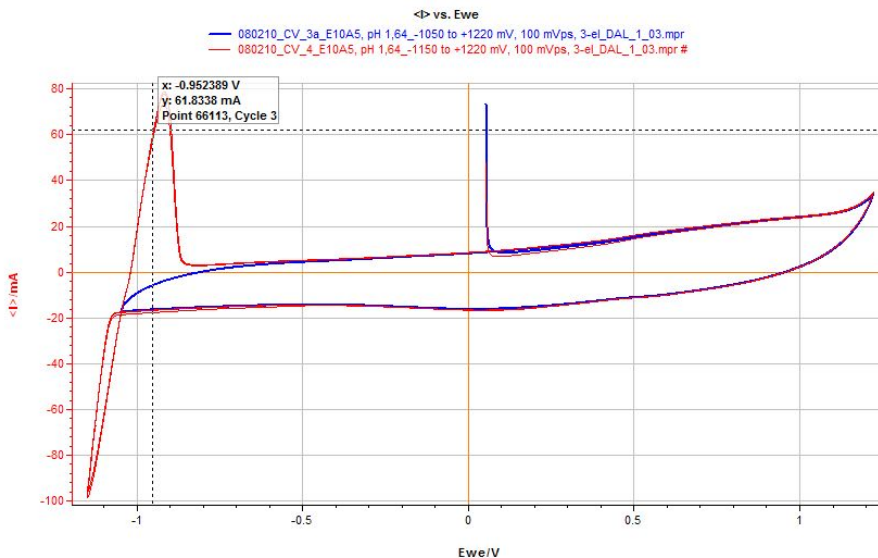


Fig. 5.9: CV scans recorded for electrolyte E10A5, at 100mV/s : inner (blue) scan: from -1.05V to $+1.22\text{V}$ vs. Ag(RE), while the external curve was obtained in the potential range from -1.05V to $+1.22\text{V}$ vs. Ag (RE).

Mettler) equipped with an InLab[©] Routine Pro pHprobe.

The described methodology will be extended for all electrolytes in our stock. Primarily, we will focus on electrolytes with a pH value relatively to the neutral pH. This means the range $2.5 < \text{pH} < 5.5$. We are, however, interested in the E020 series of strongly basic electrolytes, as well. In addition to E022, which has already been tested in open cell experiments, with graphite film WE (see table above), we will perform similar experiments on E020 and E022 listed in Table below, and some other chlorate based electrolyte from the E030 series in Table 5.2, which have not been tested, so far.

Once we down-select the electrolytes offering the largest voltage window, we utilize them in testing the real cathode material, with incorporated $\text{RuO}_2 \cdot n\text{H}_2\text{O}$. For this, we use carbon paste electrode, which served well for the preliminary ex situ investigation of various dendrimers.

We will add $\text{RuO}_2 \cdot n\text{H}_2\text{O}$ powder in 1:1 volume ratio to the carbon paste, will homogenize the mixture by stirring it with a thin spatula, and then fill with this mixture the cavity of the carbon paste electrode. The same paste could be made with $\text{RuO}_2 \cdot n\text{H}_2\text{O}$ and our activated carbon (used routinely in preparing the cathode paste of our galvanic cells) by adding the powder mixture the minimum volume of silicon oil, which still allows for the

formation of the paste, and keeping the powder together. Then, this paste would be filled in the cavity of the carbon paste electrode, and tested by CV according to the previously established procedures for carbon paste electrodes.

Electrolyte	pH (new probe)	H ₂ discharge [V vs. Ag(RE)]		H ₂ O Decomposition. [V vs. Ag (RE)]	
		C	C + RuO ₂	C	C + RuO ₂
A10A4	-0.15	-0.850		+1.220	
A10A5	1.64	-1.050	-1.000	+1.220	+1.080
E10A7 PEG6	1.66	-1.200	-1.135	+1.130	+1.080
E032A	2.05	-1.250	-1.200	+1.410	+1.410
E030A	2.26	-1.150	-1.120	+1.300	+1.400
E10A7	2.40	-1.100		+1.250	
E10A3	3.93	-1.060	-1.030	+1.120	+1.075
E031A	4.16	-1.040		+1.250	
E10A	4.54	-1.050	-1.030	+1.150	+1.100
E10A13	5.68	-1.120		+1.650	
E032	5.72	-1.200	-1.100	+1.330	+1.340
E015	5.75	-1.150	-1.125	+1.300	+1.280
NaHCO ₃	8.25	-1.350	-0.500	+1.320	+1.220
E022	14.45	-0.520		+0.450	

Tab. 5.5: Potential windows for various electrolytes.

5.6 XPS Analysis

We have analyzed a freshly made cell and a completely discharged copy of the same cell using XPS (X-Ray Photon Spectroscopy), at the Shared Instrumentation Facilities of the Dept. of Chemistry, University of Maryland in College Park. The XPS facilities are directed and used by Dr. Karen Gaskell.

XPS works by sending monochromatic x-rays to the sample and measuring the kinetic energy and number of emitted electrons. The results are given in a binding energy-vs-count of electrons detected per second. The visible peaks in a typical spectrum correspond to orbital binding energies and characteristic Auger emission energies of materials. Figure 5.10 below is an example graph taken from Wikipedia, showing the 2p-level-split of Silicon.

Some features of XPS analysis that is relevant to our particular case are listed below:

1. Some characteristic peaks of certain materials overlap. Significant in our case is the

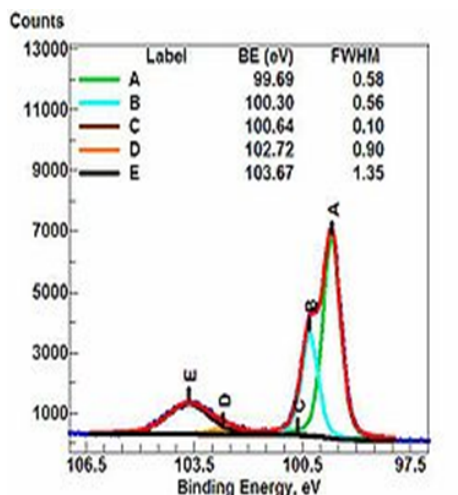


Fig. 5.10: The Si(2p) peak obtained with XPS.

overlap between C(1s) and Ru(3d). In such cases, other peaks of similar materials can be consulted for verification.

2. The place and shape of peaks can be used to deduce oxidation states of a given material, as well as to distinguish, for instance, between metallic Zn and ZnO. Metallic material peaks tend to be narrower and asymmetric.
3. It is possible to get a rough idea of the sample composition in terms of number-of-atoms ratios between different species in the sample.
4. XPS is ran in a high vacuum. Therefore, during the measurement the ruthenium oxide in the samples is probably losing its water of hydration. This is a possible phenomena to be aware of during the analysis.

5.6.1 Analysis on the Cathode Side

Figure 5.11 shows the full survey results for the “black powder” (mainly the compounded mix of ruthenium oxide and activated carbon, plus leftover solute materials from the electrolyte after the solvent has dried in the vacuum) for the new and discharged batteries.

Examining this result, several points can be immediately made:

1. Metallic zinc (Zn) is present on the cathode side even in the non-discharged (new) battery. This indicates that some Zn is immediately dissolved when the battery is

made, and that Zn^{2+} ions can travel through the standard separator we have been using (filter paper). After the discharge, the amount of Zn increases.

2. The C: Ru atomic ratio is about 12:1. From the compounding ratio of AC:RuO_x we use, we would have expected 6.7:1 if the ruthenium oxide had not been hydrated, and a higher amount since it is hydrated (but we are uncertain of the number of water of hydration). Since there is further carbon present from the elements of the electrolyte, such as ethylene glycol, the measured result there is a deviation in the expected direction.
3. Zooming on the peak shared between C1s and Ru3d shows an interesting effect of the discharge, which is also verifiable by checking the Ru3p peaks (see Figure 5.12). In the discharged battery, the peaks caused by ruthenium have almost disappeared. Since no ruthenium can be detected from samples taken from anywhere else in the battery, particularly not on the other side of the separator, one plausible conclusion is that ruthenium is being covered/coated with a material during discharge. See ahead for what can be done to verify this theory.
4. The analysis on oxidation states of ruthenium is not yet complete. Some Ru⁴⁺, consistent with the presence of RuO₂, is detectable in the new battery. However, the discharged battery does not show any relevant peak due to possible coating-over.

5.6.2 Analysis on the Anode Side

On the anode side, which is constructed by using a zinc sheet in these batteries, a white powder precipitate was available to brush off and use as the analytical sample. From our previous work, we can theorize that this was either ZnO or Zn(OH)₂. It is a relevant observation that the precipitate is present not only in the discharged cell, but also in the fresh cell, although it must be noted that the “*fresh*” cell, while never discharged, had been made several days prior to being cut and opened for sample collection. This is consistent with the observation that zinc ions have made their way over to the cathode side already in the new cell, indicating zinc dissolution.

Preliminary examination of this result leads to several conclusions:

1. There is no ruthenium and very little carbon present on this side. This is consistent with the conclusions that neither carbon nor ruthenium dioxide migrates inside the cell during use. The small amount of carbon present is very likely remains from the organic electrolyte molecules, including citric acid and ethylene glycol.
2. The only form of zinc that can be discerned is oxidized, non-metallic zinc. This can be ZnO or Zn(OH)₂. See Figure 5.14 below for a zoom-in on two characteristic Zn peaks. The exact oxidation state, and, therefore, the probable compounding, is the subject of further analysis, to be discussed ahead.

5.6.3 Further XPS Measurements and Analysis

For investigating the problem of ruthenium “*disappearing*” on the cathode side in the discharged battery, we use the depth-profiling capability of the XPS system. This capability allows the user to sputter the sample with argon ions for pitting away the top few nm of the sample, and looking at what is underneath. This way, it may be possible to both identify the oxidation states of ruthenium in the discharged sample, as well as, by noticing which materials decrease percentage-wise as the depth increases, to determine what may be coating the ruthenium paste.

We perform further detailed analysis on samples on either side to determine the exact oxidation states and more precise ratio information on the species.

In particular, with the anode side sample, deciding between ZnO and Zn(OH)₂ (or, possibly, another Zn compound) requires the performance of detailed peak-shifting and Auger parameter analyses, which are underway. These analyses will be carried out comparatively between the new and discharged samples to determine how oxidation progresses during discharge.

Finally, the discharged battery sample provided to Dr. Gaskell for analysis had actually been put through a hard discharge, consisting of several days’ worth of both terminals being shorted. We intend to carry out similar analyses on both samples at several levels (“*depths*”) of discharge, as well as on samples that have recently undergone recharging.

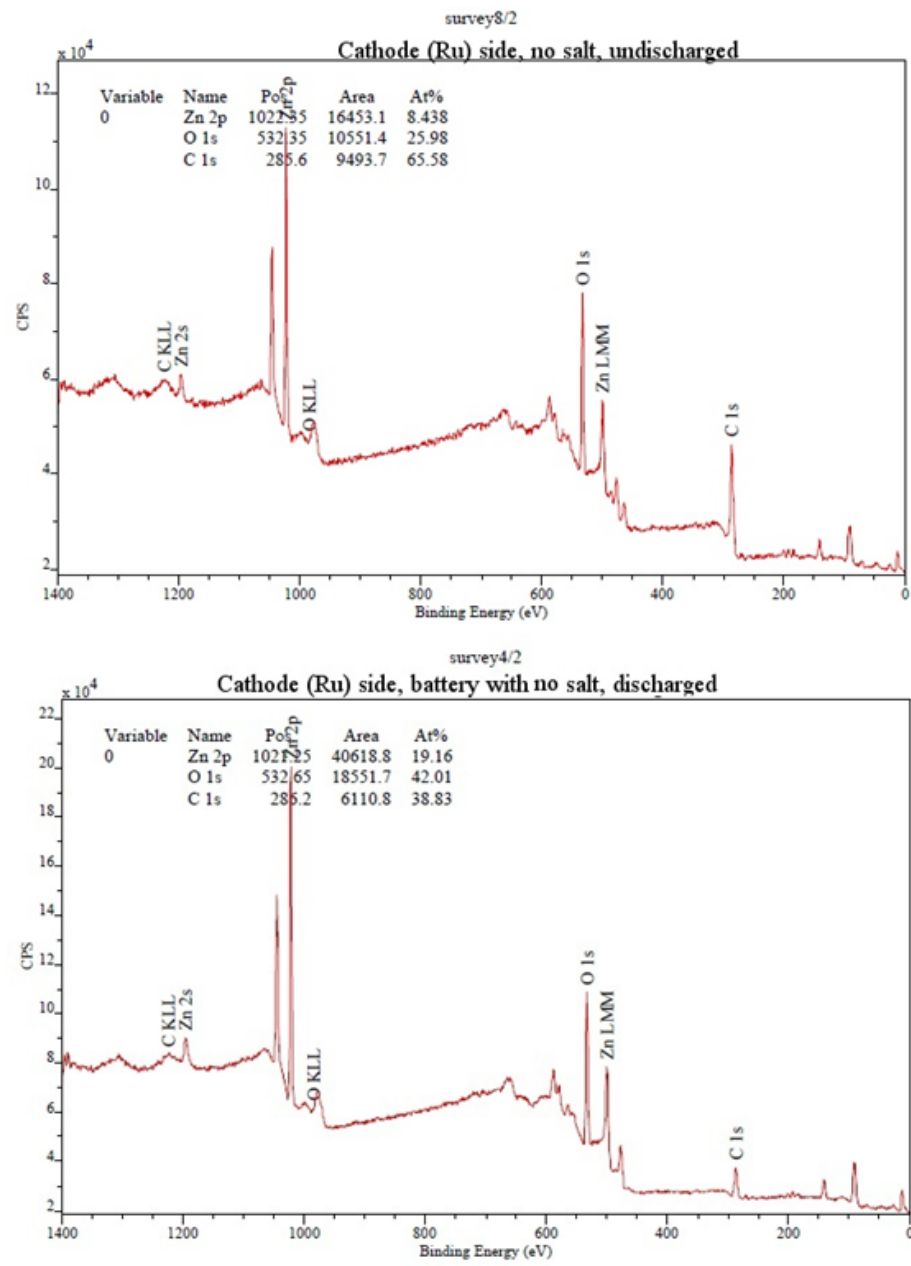


Fig. 5.11: Full XPS spectrum for cathode-side samples from undischarged (top) and discharged (bottom) batteries.

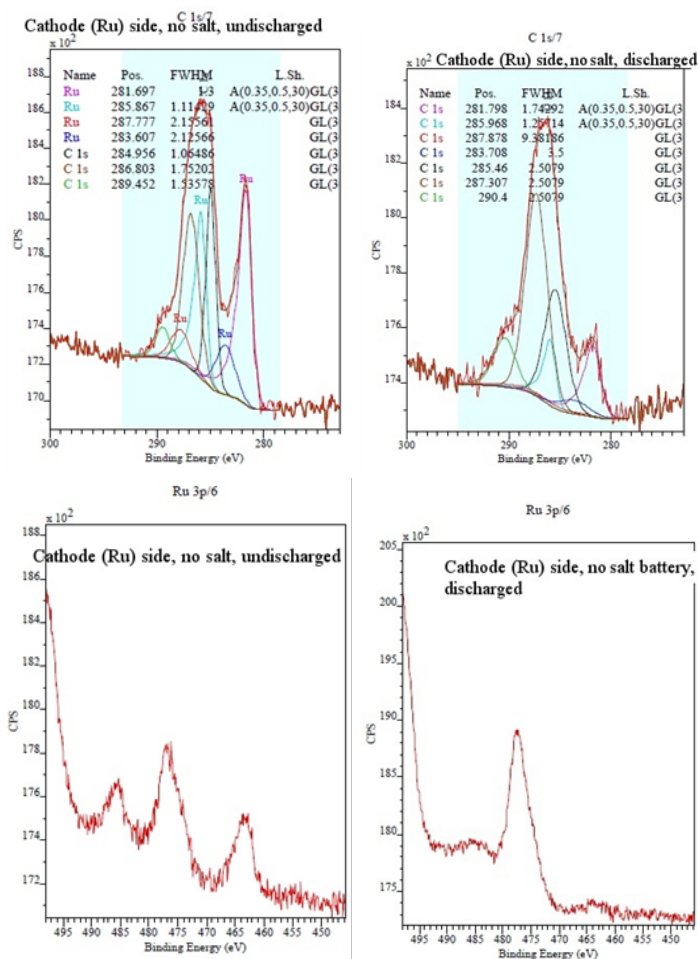


Fig. 5.12: Top: Zoom in on the C1s/Ru3d peak; left: new battery; right: discharged battery. Bottom: Zoom in on the Ru3p split peak; left: new battery; right: discharged battery. Of the four peaks visible in the bottom left graph, from left to right (higher-to-lower binding energy) the peaks are ZnAuger, Ru1p, ZnAuger, the other Ru1p. In the discharged battery graph, only the Zn peaks remain clearly visible.

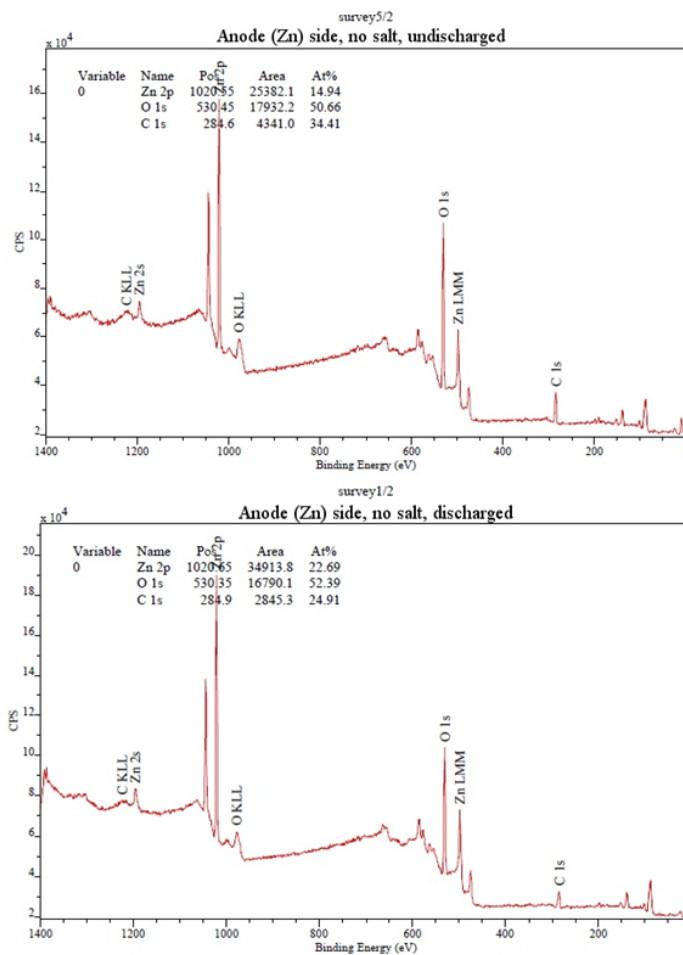


Fig. 5.13: Full XPS spectrum for anode-side (Zn) samples from undischarged (top) and discharged (bottom) batteries.

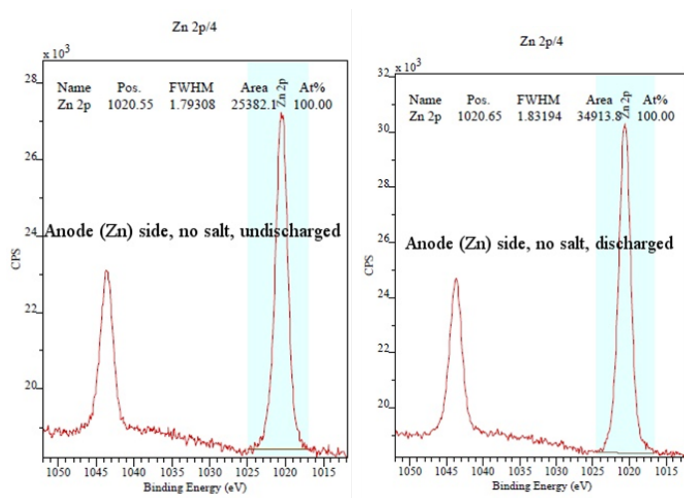


Fig. 5.14: Zoom in on the Zn 2p peaks from the new (left) and discharged (right) batteries.

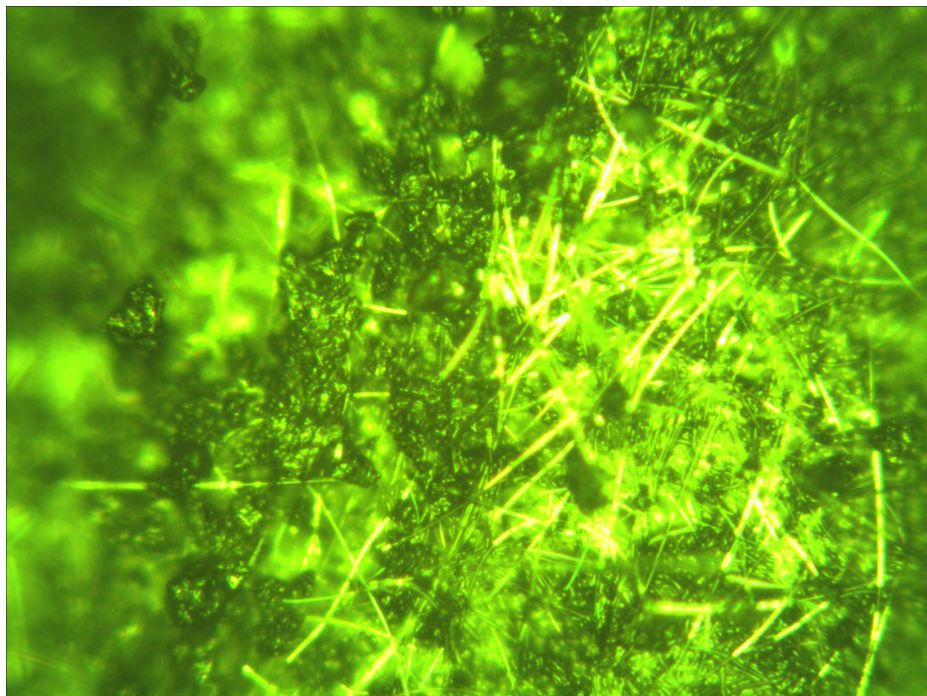


Fig. 5.15: Piece of a separator under the microscope.

Chapter 6

MANUFACTURING AND COST ANALYSIS OF Zn – RuO₂ BATTERIES

This section addresses the current state of the Zn – RuO_x battery manufacturing in terms of thickness, flexibility, cost, cycleability, and shelf life. As a result of this examination, the chapter suggests techniques for improving battery performance by controlling and optimizing these parameters. In the current state of the performance the novel ruthenium(IV) oxide cell hold the “*world record*” in terms of capacity of a flexible thin cell.

6.1 Current Stage of the Novel Ruthenium(IV) Oxide Cells

6.1.1 Thickness

The thickness of the batteries depends on the material used for electrodes, separators, current collectors, and on the thickness of the packaging material, as well. Our intent was to optimize these parameters, such that highest possible capacity of the cell is reached. Currently, all the batteries manufactured on the lab scale are made with 0.65mm thick zinc plate, given its low cost. These materials are used for manufacturing kitchen counter tops, and the material has proven suitable for devising battery anodes, as it consists of 99.99% pure zinc. A graphite sheet of 0.13mm thickness is used as the cathode current collector. These materials are utilized in most of the batteries, since they offer the best performance. For a regular battery, the separator thickness is of 0.350mm, which enables for the highest capacity, as described in section 5.3. Using the three main components above plus the packaging, the nominal thickness of the battery becomes 1.5mm. One should note

here that these batteries can also be made with thinner zinc, as thin as 0.0762mm or even 0.0254mm . The batteries equipped with thin zinc foils delivers, however, charge capacity, as a consequence of faster corrosion of the zinc. section 5.3 of this thesis discussed different cathode current collector that can possibly be used instead of graphite sheet. As explained in section 5.3, the tested materials provide less charge capacity; therefore, to the present they have not been used as a replacement of graphite sheets.

6.1.2 Capacity

We have shown that when RuO_x is used with appropriate electrolyte, it continues operating as a cathode material even after it has been reduced from Ru(IV) to lower oxidation states. Its extended job is most likely the result of catalyzing hydrogen ion (or water) reduction at the $\text{RuO}_x/\text{electrolyte}$ interface [79].

We have demonstrated cell capacities as high as $33.35\text{mAh}/\text{cm}^2$ for Zn-RuO_x batteries. This capacity has been achieved by using thick zinc (0.65mm), graphite sheet, and fiber-glass filter paper with the pH set to the slightly acidic value of pH2.43. Battery made with same material but thinner zinc (0.0762mm) delivered the lower capacity of $16\text{mAh}/\text{cm}^2$, because of zinc corrosion. Table 6.1 below compares the capacity of the Zn – RuO_x cell with several competitor batteries. As revealed by the listed values, the FlexEl battery exhibits the highest charge capacity relative to other non-rechargeable flexible batteries[79, 80, 81, 82].

	RuO ₂ /Zn	RuO ₂ /Zn	Enfucell	Enfucell	Power Paper	Blue Spark
Nominal voltage [V]	1.4	1.4	1.5	3	1.5	1.5
Nominal capacity (mAh/cm^2)	16	33.35	2.1	0.4	1.2	1.3

Tab. 6.1: The Capacity Comparison of Non-Rechargeable Flexible Batteries.

It can be observed that the Zn – RuO_x battery has one order of magnitude greater specific surface capacity (in mAh/cm^2) as compared to other thin-film, non-rechargeable flexible batteries. The record for rechargeable, flexible, thin-film batteries is clearly held by the FlexEl galvanic cell.

6.1.3 Costs

Ruthenium and zinc are the most expensive components of the proposed battery. Therefore, we explored possibilities for reducing these costs. We expect these costs to be significantly lower for large scale production.

Ruthenium Costs

Hydrated Ru(IV) oxide is the main component of the proposed battery; this is a very expensive compound. Due to its high cost, it has largely been ignored as a viable candidate for battery cathode material. As explained in section 3.2, the paste used in the battery is a mixture of RuO_x and activated carbon (AC); by “*diluting*” Ru(IV) oxide with AC, we reduce the cost of the ruthenium significantly. Also, utilizing nano-coating technologies, we can reduce to a significant extent the amount of ruthenium incorporated in our cells. This technique has been examined, but it represents an approach beyond the tasks of this Thesis.

Zinc Costs

Zinc is the second most expensive component of the novel Zn – RuO_x batteries. What makes this metal expensive is the need for shaping it into a very thin zinc foil. The cost of zinc increases noticeably as the metal sheets become the thinner and thinner. As explained previously, in present we are using 0.65mm thick zinc plates, which enable low expense laboratory scale battery manufacturing. Znplate is noticeably cheaper than thin zinc foil. The materials cost $\$0.005$ per square centimeter. Comparably, the cost of thin zinc foil is almost 50 times more expensive, of approximately $\$0.23$ per square centimeter. Therefore, there is a need for identifying a thinning technology, which can reduce the thickness of the 0.75mm zinc plate, while keeping its cost low.

6.1.4 Cycle Life

Studies show that ruthenium is the best candidate for the non-rechargeable flexible batteries. It can also be used in rechargeable batteries. We have demonstrated more than 800 cycles

with *1min* discharges into a 10Ω load followed by *3min* charging as shown in section 5.4. Over the first 30s these discharges source approximately $100mA$ for a $4cm^2$ cell, when the discharge occurs at the average voltage of $1V$. Cycle life at deep discharges is currently limited by the hydrogen evolution, and the discussion of the latter phenomenon does not represent the scope of this thesis. High internal resistance of a cell and cell dry-out are two important factors, which limit the cycleability of the cell. Formation of zinc oxide can also affect the cycleability of a cell. Details about cycling of $Zn - RuO_x$ batteries have been provided in subsection 5.4.1.

6.1.5 Safety and Sustainability

Most of the batteries currently commercialized are lithium-ion based. Lithium like all alkali metals, is highly reactive and flammable. Therefore, these batteries are not environmentally friendly, and can be extremely harmful. The RuO_x cell chemistry is inherently non-toxic, and environmentally benign. Zinc is nontoxic, being used in anti-fire medicine. Acidity of the electrolytes used to make batteries is comparable to that of a salad dressing, so it will not cause any harm to the human body.

Chapter 7

ACCOMPLISHMENTS AND FUTURE CONSIDERATIONS

7.1 Summary of Main Accomplishments

The main focus of this Thesis was to design and manufacture ultrathin galvanic cells that can comply with a variety of form factors and electronic system packages. Such cells are in great demand, as they show promise for flexible electronic systems. Described is a flexible, high energy density galvanic cell, based on hydrated ruthenium (IV) oxide-zinc electrodes, which utilizes $\text{RuO}_2 \cdot n\text{H}_2\text{O}$ nanoparticles, in amounts that are not cost-prohibitive. So far, Ru(IV) oxide was utilized almost exclusively in supercapacitors, their possible application as a cathode material in batteries being almost completely neglected. Therefore, our approach of building battery systems the topic of this Thesis represents a breakthrough scientific novelty. The obtained battery is suitable for use in a number of environments, is non-toxic, environmentally friendly, and, being based on aqueous electrolytes, it is safe in operation. It can be optimized for volume manufacture at low cost. As it functions at much lower cell voltage than Li-ion batteries, it can be recharged remotely, at conveniently low voltage, by harvesting, for example, radio-frequency (RF) energy.

The first chapter of the Thesis is a literature review, which summarizes the data from public domain on thin-film Li-ion batteries, the use of hydrated ruthenium (IV) oxide in supercapacitors, describes the relatively few commercially available thin-film battery systems, and provides insight in hybrid power systems, consisting of a galvanic cell and a supercapacitor.

Next, battery operation is explained, with sections dedicated to thermodynamic considerations and the kinetics of the galvanic cell. Attention is paid to the effect exerted by various electrolytes and to the cell separators.

chapter 3 takes a close look into the fabrication and characterization of the novel Zn – RuO₂ cells. Described are problems and technical solutions for the anode and the cathode half-cell, the proper choice of electrolyte, of the cell separator, and of current collectors.

Specific investigation techniques and the needed instrumentation are addressed in chapter 4, where the electrochemical techniques are grouped into the ones performed in 3-electrode geometry and others, which can be carried out in 2-electrode geometry. Discussed are cyclic voltammetry, open circuit voltage vs. time measurements, charge/discharge studies (including charging at constant current or at constant voltage, and discharge at constant external load or at constant current, i.e., by chronopotentiometry). Additional tests disclosed in this chapter include cycling experiments, shelf life/self-discharge examination, and internal resistance measurements.

The most significant experimental results are described in a systematic manner in chapter 5. In order to learn more about the mechanism of the electroactive processes that drive the galvanic cells, the investigation went beyond the Electrochemical testing, the cathode and anode materials being analyzed by XPS (subsection 5.6.3).

Current stage of the novel zinc-ruthenium (IV) oxide cell is evaluated in chapter 6, where the most important parameters are discussed in separate sections, namely: thickness of the device, capacity of the galvanic cell, and the fabrication costs. In present this cell demonstrates a specific capacity of over $35mAh/cm^2$, which is, so far, the largest reported for thin-film cells. Also, its cycle life of up to 200 charge/discharge cycles is very promising for use as a secondary galvanic cell.

My last section takes a look on the prospective of the described galvanic cell. It describes briefly research strategies and research plans toward improving the existing system, mainly via increasing its charge capacity and its cycle life.

7.2 Future Considerations

Optimization of each battery component is needed. Below are the suggested technologies that can help the performance of the battery.

7.2.1 Anode Optimization

To date, the bulk of our research has focused on Zn as an anode material, but other metals may be considered as candidates. Although, primary experiments have demonstrated favorable performance of zinc anodes, I plan performing a broader exploration of anode materials, to confirm that zinc is the most suitable choice for pursuing further developments. Assuming that we will be able to confirm the choice of zinc as an anode material, we are going to explore techniques for low-cost thin zinc manufacturing. Additionally, we will want to explore a variety of compounds added to zinc for lowering its internal resistance and improving its cycling ability through reduction in shape change and corrosion.

7.2.2 Cathode Optimization

A variety of cathode materials have been explored for their ability to collect electrons, and to provide low resistance current collectors to the electrolytic medium. In addition, there is a need for new approaches for creating ultrathin cathode current collectors. Ultrathin carbon structures have been already used in other applications [83, 84]. One common method is to use a fluid filtration and drying procedure, similarly to the one utilized in paper manufacturing. The result is commonly referred to as "*buckeye*". Several companies offer this as a commercial product, made of carbon nanotube, where the thickness of the paper determines its cost [84]. section 5.2 of this Thesis shows the result obtained with buckeye paper having the thickness of $0.1\mu m$. Our goal is, however, to be able to reduce the thickness even further. Experiments need to be done for investigating the performance of the battery, when thinner buckeye paper is used. We plan on exploring commercially available thin-film carbon conductors for our initial experiments and, if successful, we will create and incorporate in our cells even thinner conductors.

Other considered techniques are various coating technologies. This approach not only

helps for thinning the battery structure, but also enables for reducing the amount of hydrated ruthenium oxide, which needs to be used per square centimeter of the battery. The goal is to coat ruthenium and activated carbon compounds on thin current collectors. Further investigation needs to be done for identifying an appropriate technology, which can coat powders on a conductive substrate, such that the resulting structure should have a low Ohmic resistance.

7.2.3 Electrolyte Optimization

There is a need for exploring the full range of pH values, which may allow for maximizing the cell capacity and cycleability, as well. We are going to explore the possible recipes for electrolytes that provide the highest capacity, while increasing the shelf life.

The next very important step in optimizing the electrolyte is switching to gel-type electrolytes. Use of such electrolytes may offer important advantages for ease-of-manufacturing and battery lifetimes, as well as preventing the increase of internal resistance, as the unwanted result of hydrogen evolution. Also, cycle life may be improved, by reducing dendrite formation. Lastly, utilizing gel type electrolytes that can be cast directly onto the surface of one of the battery electrodes eliminates the need for a cell separator. This renders the battery design simpler and more efficient. Although, we were able to prepare several alkaline gel electrolytes, the results obtained with these batteries were not as good as with liquid electrolytes. Therefore, we are going to further investigate the technique for preparing gel electrolytes, such that battery performance is maintained at its highest level.

BIBLIOGRAPHY

- [1] Selvapathy, P., Madhavan, S.D., “*Risk Assessment of used Household Batteries in the Municipal Solid Waste - A Case Study*,” 2003. Workshop on Sustainable Landfill Management, December, 3-5, 2003, Chennai, India, pp. 219-224.
- [2] Scrosati, B. “*Battery technology - Challenge of Portable Power*,” 1995. *Nature*, 373 (6515), pp. 557-558.
- [3] “*Basic Research Needs for Electrical Energy Storage*,” 2007. Report of the Basic Energy Sciences Workshop for Electrical Energy Storage, April 2-4, 2007. Office of Basic Energy Sciences, Department of Energy, July 2007.
- [4] “*World Batteries to 2012 - Market Research, Market Share, Market Size, Sales, Demand Forecast, Market Leaders, Company Profiles, Industry Trends*,” Freedonia Industry Study #: 2375, <http://www.freedoniagroup.com/> (Sept. 21, 2010).
- [5] Lowy, D.A., “*An Electrochemical Journey at the Nano Scale*,” 2009. Ed. Casa Stiintei, Cluj, pp. 4-5.
- [6] Bates, J.B., Dudney, N.J., Lubben, D.C., et al. “*Thin-Film Rechargeable Lithium Batteries*,” 1995. *J. Power Sources*, 54 (1), pp. 58-62.
- [7] West, W.C., Whitacre, J.F., White, V., Ratnakumar, B.V. “*Fabrication and Testing of All Solid-State Microscale Lithium Batteries for Microspacecraft Applications*,” 2002. *J. Micromech. Microeng.*, 12 (1), pp. 58-62.
- [8] Buchmann, I. “*Batteries in Portable World. Handbook on Rechargeable Batteries for Non-Engineers*,” 2001. Cadex Electronics Inc.
- [9] “*Smart Nanobattery Makes History*,” 2008. *Am. Ceramic Soc. Bull.*, 87 (5), pp. 34-34.

- [10] “*Smart Nanobattery Designed to Be $\dot{\iota}$ Green.j*”, 2007. Am. Ceramic Soc. Bull., 86 (3), pp. A12-A12.
- [11] Barak, M. “*Primary Batteries - Introduction,*” 1981. In: Bockris, J.O’M., Conway, B.E., Yeager, E., White, R.E. (Editors), “*Comprehensive Treatise of Electrochemistry,*” Plenum Press, New York, London, p. 193.
- [12] Sacrosati, B. “*Paper Powers Battery Breakthrough,*” 2007. Nature Nanotech., 2 (10), pp. 598-599.
- [13] Souquet, J.L., Duclot, M., “*Thin-film lithium batteries,*” 2002. Solid State Ionics, 148 (3-4), pp. 375-379.
- [14] Dudney, N. J., Neudecker B.J. “*Solid state thin-film lithium battery systems,*” 1999. Current Opinion in Solid State & Materials Science, 4, pp. 479-482.
- [15] Pushparaj, V.L., Shaijumon, M.M., Kumar, A., Murugesan, S., Ci, L., Vajtai, R., Linhardt, R.J., Nalamasu, O., Ajayan, P.M., “*Flexible energy storage devices based on nanocomposite paper,*” 2007. Proc. National Acad. Science USA, 104 (34), pp. 13574-13577.
- [16] Bates, J.B., Dudney, N.J., Neudecker, B., Ueda, A., Evans, C.D. 2000, “*Thin-film lithium and lithium-ion batteries,*” Solid State Ionics, 135, pp. 33-36.
- [17] Dudney, N.J. “*Solid-state thin-film rechargeable batteries,*” 2005. Materials Science & Engineering B, 116, pp. 245-249.
- [18] Dunn, B., Long, J.W., Rolison, D.R., “*Rethinking Multifunction in Three Dimensions for Miniaturizing Electrical Energy Storage,*” 2008. The Electrochemical Society Interface, Fall issue, pp.49-53.
- [19] Wang, J.-Z., Chou, S.-L., Liu, H., Wang, G.X., Zhong, C., Chew, S.Y., Liu, H.K., “*Highly flexible and bendable free-standing thin-film polymer for battery application,*” 2009. Materials. Letters, 63 (27), 2352-2354.

- [20] Neudecker, B.J., Dudney, N.J., Bates, J.B., “*Lithium-Free Thin-Film Battery with In Situ Plated Li Anode*,” J. Electrochem. Soc., 2000. 147 (2), pp. 517-523.
- [21] Neudecker, B.J., Zuhr, R.A., Bates, J.B., “*Lithium silicon tin oxynitride (Li₂SiTON): high-performance anode in thin-film lithium-ion batteries for microelectronics*,” 1999. J. Power Sources, 81-82, pp. 27-.
- [22] Wang, B., Bates, J.B., Hart, F.X., Sales, B.C., Zuhr, R.A., Robertson, J.D., “*Characterization of Thin-Film Rechargeable Lithium Batteries with Lithium Cobalt Oxide Cathodes*,” 1996. J. Electrochem. Soc., 143 (10), pp. 3203-3213.
- [23] Lee, S.H., Liu, P., Tracy, C. E., Benson, D.K., “*All-Solid-State Rocking Chair Lithium Battery on a Flexible Al Substrate*,” 1999. Electrochem. Solid-State Lett., 2 (9), pp. 425-427.
- [24] Bates, J.B., Dudney, N.J., Lubben, D.C., Gruzalski, G.R., Kwak, B.S., Yu, X., Zuhr, R.A. “*Thin-film rechargeable lithium batteries*,” 1995. J. Power Sources, 54, pp. 58-62.
- [25] Young-Shin Park, Se-Hee Lee, Byung-Il Lee, and Seung-Ki Joo, 1999. “*All-Solid-State Lithium Thin-Film Rechargeable Battery with Lithium Manganese Oxide*,” Electrochem. Solid-State Lett., 2 (2), pp. 58-59.
- [26] Southee, D., Hay, G.I., Evans, P.S.A., Harrison, D.J., “*Lithographically Printed Voltaic Cells - A Feasibility Study*,” 2007. Circuit World, 33 (1), pp. 31-35.
- [27] Hiralal, P., Imaizumi, S., Unalan, H.E., Matsumoto, H., Minagawa, M., Rouvala, M., Tanioka, A., Amaratunga, G.A. “*Nanomaterial-Enhanced All-Solid Flexible Zinc-Carbon Batteries*,” 2010. ACS NANO, 4 (5), pp. 2730-2734.
- [28] Xu, J.J., Ye, H., Huang, J. “*Novel Zinc Ion Conducting Polymer Gel Electrolytes Based on Ionic Liquids*,” 2005. Electrochem. Comm. 7 (12), pp. 1309-1317.
- [29] Narayanan, N.S.V., Ashokraj, B.V., Sampath, S. “*Ambient Temperature, Zinc Ion-Conducting, Binary Molten Electrolyte Based on Acetamide and Zinc Perchlorate: Application in Rechargeable Zinc Batteries*,” 2010. J. Colloid & Interface Science, 342 (2), 505-512.

- [30] Narayanan, N.S.V., Ashokraj, B.V., Sampath, S. “*Physicochemical, Electro chemical, and Spectroscopic Characterization of Zinc-Based Room-Temperature Molten Electrolytes and Their Application in Rechargeable Batteries,*” 2009. J. Electrochem. Soc., 156 (11), A863-A872.
- [31] Simon, S., Lifton, V., Allen, F. “*Extending the Life of Wireless Networks Using the Smart NanoBattery. White Paper,*” 2008. mPhase Technologies, Inc. / AlwaysReady, Inc., Little Falls, New Jersey, September 2008.
- [32] Krupenkin, T.N., Taylor, J.A., Kolodner, P., Hodes, M. “*Electrically Tunable Superhydrophobic Nanostructured Surfaces,*” 2005. Bell Labs Tech. J. 10 (3), pp. 161-170.
- [33] Krupenkin, T.N., Taylor, J.A., Wang, E.N., Kolodner, P., Hodes, M., Salamon, T.R. “*Reversible Wetting-Dewetting Transitions on Electrically Tunable Superhydrophobic Nanostructured Surfaces,*” 2007. Langmuir, 23 (18), pp. 9128-9133.
- [34] Krupenkin, T.N., Taylor, J.A., Schneider, T.M., Yang, S. “*From Rolling Ball to Complete Wetting: The Dynamic Tuning of Liquids on Nanostructured Surfaces,*” 2004. Langmuir, 20 (10), pp. 3824-3827.
- [35] Ahuja, A., Taylor, J.A., Lifton, V., Sidorenko, A.A., Salamon, T.R., Lobaton, E. J., Kolodner, P., Krupenkin, T.N. “*Nanonails: A Simple Geometrical Approach to Electrically Tunable Superhydrophobic Surfaces,*” 2008. Langmuir, 24 (1), pp. 9-14.
- [36] Krupenkin, T.N., Mandich, M.L., Taylor, J.A. 2005. EP 1591415A2, 2005. US 2005269743A1, 2005. JP 05349558A, 2005. DE 6005000397E, 2005. DE 6005000397T2, 2005. US 20057323033B2.
- [37] Brazier, A., Dupont, L., Dantras-Laffont, L., Kuwata, N., Kawamura, J., Tarascon, J.-M. “*First Cross-Section Observation of an All Solid State Lithium-Ion ”Nanobattery” by Transmission Electron Microscopy,*” 2008. Chem. Mater., 20 (6), pp. 2352-2359
- [38] Lifton, V.A., Taylor, J.A., Vyas, B., Kolodner, P., Cirelli, R., Basavanahally, N., Papazian, A., Frahm, R., Simon, S., Krupenkin, T. “*Superhydrophobic Membranes with*

- Electrically Controllable Permeability and Their Application to "Smart" Microbatteries,*" 2008. Appl. Phys. Lett., 93, Paper #043112.
- [39] Hilder, M., Winther-Jensen, B., Clark, N. B. "*Paper-Based, Printed Zinc-Air Battery,*" 2009. J. Power Sources, 194 (2, Sp. Iss.), pp. 1135-1141.1.40
- [40] Dennler G., Bereznev, S., Fichou, D., Holl, K., Ilic, D., Koeppe, R., Krebs, M., Labouret, A., Lungenschmied, C., Marchenko, A., Meissner, D., Mellikov, E., Mot, J., Meyer, A., Meyer, T., Neugebauer, H., pik A., Sariciftci, N.S., Taillemite, S., Whrle T. "*A self-rechargeable and flexible polymer solar battery,*" 2007. Solar Energy, 81 (8), pp. 947-957.
- [41] Park, B.-O., Lokhande, C.D., Park, H.-S., Jung, K.-D., Joo, O.-S. "*Performance of supercapacitor with electrodeposited ruthenium oxide film electrodes-effect of film thickness,*" 2004. J. Power Sources, 134, pp. 148-152.
- [42] Yoon, Y.S., Cho, W.I., Lim, J.H., Choi, D.J. "*Solid-state thin-film supercapacitor with ruthenium oxide and solid electrolyte thin-films,*" 2001. J. Power Sources, 101 (1), pp. 126-129.
- [43] Choi, S.H., Kim. J., Yoon, Y.S. "*Fabrication and characterization of a SnO₂-RuO₂ composite anode for a hybrid thin-film battery,*" 2005. Metals & Materials International, 11 (1), 77-83.
- [44] Kim, I.H., Kim, K.B. "*Ruthenium oxide thin-film electrodes for supercapacitors,*" 2001. Electrochem. Solid State Lett., 4 (5), A62-A64.
- [45] "Battery" in wikipedia: http://en.wikipedia.org/wiki/Battery%28electricity%29#Primary_batteries
- [46] Dell, R.M. Rand D.A.J. "Understanding Batteries," Royal Society of Chemistry, 2001, PP. 9-25
- [47] Barak, M. "Primary batteries - Introduction," in: Bockris, J. Conway, B. Yeager, E. White, R. (Eds.) "Comprehensive Treatises of Electrochemistry,"

- [48] Zumdahl S.S. Zumdahl S.A. "Chemistry," 2007. 7th Edition, Houghton Mifflin Company, Boston Newyork, pp. 891-821.
- [49] "Standard Electrode Potential" in wikipedia: http://en.wikipedia.org/wiki/Table_of_standard_electrode_potentials
- [50] Bard, A.J., Faulkner, L.R. "Electrochemical Methods. Fundamentals and Applications,". 2001. 2nd edition, John Wiley & Sons, Inc., New York, Chichester, Weinheim, Brisbane, Singapore, Toronto. pp. 92. 100-106.
- [51] Kordesch, K. (1981) Electrochemical energy storage. In Comprehensive Treatise of Electrochemistry. Vol. 3: Electrochemical Energy Conversion and Storage (eds. Bockris, J.O'M., Conway, B.E., Yeager, E. and White, R.E.) pp.202.139-141., Plenum Press, New York, London.
- [52] Kissinger, P.T., Preddy, C.R., Shoup, R.E., Heineman, W.R. "Fundamental Concepts of Analytical Chemistry. In Laboratory Techniques in Electroanalytical Chemistry," 1996 (Eds. Kissinger, P.T., Heineman, W.R.) 2nd edition, Marcel Dekker, New York, Basel, pp.37-38.
- [53] Rocchini, G. "Corrosion rate monitoring by the Linear-polarization method," 1993. Corrosion Science, 34 (12), pp. 2031-2044.
- [54] Rocchini, G. " The influence of the potential sweep rate on the computation of the polarization resistance," 1996. Corrosion Science, 38 (12), pp. 2095-2109.
- [55] Rocchini, G. "Experimental verification of the validity of the linear polarization method," 1997. Corrosion Science, 39 (5), pp. 877-891.
- [56] Zhu, J.; Cheng, F.Y.; Tao, Z.; Chen, J. (2008) Electrocatalytic methanol oxidation of Pt_{0.5}Ru_{0.5-x}Sn_x/C (x=0-0.5). J. Phys. Chem. C 112(16), 6337-6345.
- [57] Eguiluz, K.I.B., Salazar-Banda, G.R., Miwa, D., Machado, S.A.S., Avaca, L.A. "Effect of the catalyst composition in the Pt-x(Ru-Ir)(1-x)/C system on the electro-oxidation of methanol in acid media," 2008. J. Power Sources 179 (1), pp. 42-49.

- [58] Innocente, A.F., Angelo, A.C.D. "Hydrogen oxidation on ordered intermetallic electrodes covered with CO," 2008. *J. Power Sources* 175(2), pp. 779-783.
- [59] Sieben, J.M., Duarte, M.M.E., Mayer, C.E. "Supported Pt and Pt-Ru catalysts prepared by potentiostatic electrodeposition for methanol electrooxidation," 2008. *J. Appl. Electrochem.* 38(4), pp. 483-490.
- [60] Salazar-Banda, G.R., Suffredini H.B., Calegaro, M.L., Tanimoto, S.T., Avaca, L.A. "Sol-gel-modified boron-doped diamond surfaces for methanol and ethanol electrooxidation in acid medium," 2006. *J. Power Sources* 162(1), pp. 9-20.
- [61] Kim, Y.J., Hong, W.H., Woo, S.I., Lee, H.K. "Analysis of the polarization of a direct methanol fuel cell using a pseudo-reversible hydrogen reference electrode," 2006. *J. Power Sources* 159(1), pp. 491-500.
- [62] Thompson, E.L., Jorne, J., Gasteiger, H.A. "Oxygen reduction reaction kinetics in subfreezing PEM fuel cells," 2007. *J. Electrochem. Electrochem. Soc.* 154 (8), pp. B783-B792.
- [63] Chirkov, Y.G., Rostokin V.I. "Hydrophobized oxygen cathode of a fuel cell with a liquid electrolyte: Calculating overall currents and thicknesses," 2007. *Russian J. Electrochem.* 43 (2), pp. 146-156.
- [64] Liu, D., Case, S. "Durability study of proton exchange membrane fuel cells under dynamic testing conditions with cyclic current profile," 2006. *J. Power Sources*, 179 (1), pp. 42-49.
- [65] Bockris, J. O'M., Reddy, A.K.N. "*Modern Electrochemistry. Ionics*," 1998. Second edition, Plenum Press, New York and London, Vol. 1, pp. 13,454-456.
- [66] Linden, D., Reddy, T.B. (Eds.) "*Handbook of Batteries*," 2002. Third edition, McGraw-Hill, New York, Chicago, , Toronto, pp. 8.15.
- [67] FlexEl LLC. "Novel Ultra-High Capacity PHEV battery," Internal Technical Documentation, College Park, MD. 2010

- [68] FlexEl LLC. "Novel Ultra-High Capacity PHEV battery," Internal Technical Documentation, College Park, MD. 2010
- [69] "Battery" in wikipedia: <http://en.wikipedia.org/wiki/Ruthenium>
- [70] Barak, M. "Primary batteries - Introduction," in: Bockris, J. Conway, B. Yeager, E. White, R. (Eds.) "Comprehensive Treatises of Electrochemistry," pp.202-205.
- [71] Linden, D., Reddy, T.B. (Eds.) "*Handbook of Batteries*," 2002. Third edition, McGraw-Hill, New York, Chicago, , Toronto, pp.8-23.
- [72] S.K. Toh, D.G. McCulloch, J. Du Plessis, P.J.K. Paterson, A.E. Hughes, D. Jamieson, B. Rout, J.M. Long and A. Stonham, *Surface Rev. Lett.* 10 (2003), 365.
- [73] Bard, A.J., Faulkner, L.R. "Electrochemical Methods. Fundamentals and Applications,". 2001. 2nd edition, John Wiley & Sons, Inc., New York, Chichester, Weinheim, Brisbane, Singapore, Toronto. pp. 92. 100-106.
- [74] "Potentiostats" in BioLogic: <http://www.bio-logic.info/potentiostat/brochures/20071123%20-%20MRes%20-%20VMP3.pdf>
- [75] BioLogic Science Instruments. "EC-Lab Software User's Manual," Version 9.9, France, 2010
- [76] Dell, R.M. Rand D.A.J. "Understanding Batteries," Royal Society of Chemistry, 2001, P. 38
- [77] Zhang, X.G. "Corrosion and electrochemistry of zinc," 1996. Plenum Press, New York, pp. 385-389.
- [78] Internal Resistance(IR) in Energizer: <http://data.energizer.com/PDFs/BatteryIR.pdf>
- [79] FlexEl LLC. "Novel Ultra-High Capacity PHEV battery," Internal Technical Documentation, College Park, MD. 2010
- [80] Power Paper Batteries in: <http://www.powerpaper.com/>
- [81] Blue Spark battery products in: <http://www.bluesparktechnologies.com/2.1.0.cfm>

[82] Enfucell batteries in: <http://www.enfucell.com/>

[83] Long, J.W. Rolison, D.R.” Carbon nanoarchitectures with ultrathin, conformal polymer coating for Electrochemical capacitors,” US patent 7672114

[84] ”Buckeye Composites,” 2010 in: <http://www.buckeyecomposites.com/>